Ocean Engineering 250 (2022) 111008

Contents lists available at ScienceDirect

Ocean Engineering

journal homepage: www.elsevier.com/locate/oceaneng

# The influence of damage breach sampling process on the direct assessment of ship survivability

Francesco Mauro *, Dracos Vassalos

*The Maritime Safety Research Centre, Department of Naval Architecture, Ocean and Marine Engineering (NAOME), University of Strathclyde, 100 Montrose St., Glasgow, G4 0LZ, Scotland, UK*

ARTICLE INFO

*Keywords:*
Damage stability
Non-zonal approach
Sampling methods
Monte Carlo method

ABSTRACT

The current damage stability regulatory framework for passenger and dry cargo ships allows addressing vessel survivability after flooding due to collisions with probabilistic requirements. This methodology also applies to other hazards responsible for the flooding of a ship such as bottom and side groundings. Traditionally, the application of Monte Carlo sampling of pertinent distributions allows for assessing ship survivability. Such a method introduces randomness in the process, leading to a dispersion of the attained survivability index within multiple sets of generated damages. The present work investigates sampling methods alternative to Monte Carlo, based on Latin Hypercube and Randomised Quasi-Monte Carlo processes. The sampling methods application for collisions, side and bottom groundings on a reference barge available in the literature for benchmark purposes shows that the Randomised Quasi-Monte Carlo method based on multidimensional Sobol sequences grants lower dispersion of the final survivability index data within samples of equivalent size. Finally, the application on a sample cruise ship of Monte Carlo and Randomised Quasi-Monte Carlo methods highlights the possibility to reduce the number of damage breaches necessary to evaluate the survivability index within an engineering confidence interval, thus improving accuracy and efficiency in the amplification of probabilistic damage stability methods by the industry.

## 1. Introduction

The existing regulation provided by SOLAS (Safety of Life at Sea) for ship survivability after flooding accidents considers only collisions hazards (Chapter II-1 in SOLAS IMO, 2020). More than sixty years of developments (from Wendel (1960) studies to SOLAS2020 (IMO, 2017) regulation) led to a probabilistic framework based on the calculation of the probability of flooding a group of compartments (the so-called $p$ factors) and the consequent survivability (the $s$ factors). The determination of $p$ factors derives from the description of collision damage characteristics with dedicated marginal distributions, derived from the HARDER project (Lützen, 2001, 2002; Papanikolaou and Eliopoulou, 2008) and amended in SOLAS2009 (IMO, 2006) probabilistic framework. Probability of survival stems from the static GZ curve of the damaged ship.

However, collisions are not the only possible flooding hazard for a ship, especially for passenger ships. Notably, side and bottom groundings constitute much more significant hazards than collisions (Papanikolaou et al., 2004; Zaraphonitis et al., 2015). SOLAS regulation has no direct implementation of such hazards; it only refers to generic deterministic requirements. Therefore, there is an imbalance between the collision framework complexity and accuracy and the treatment of other damages. Several studies in the GOALDS Project provide the basis for a probabilistic framework for bottom damages (Bulian and Francescutto, 2010), extended during EMSA (Zaraphonitis et al., 2015; Bulian et al., 2016) and eSAFE (Zaraphonitis et al., 2017; Bulian et al., 2020) Projects to a complete framework for collisions, bottom and side groundings (Bulian et al., 2019). Such a probabilistic framework for ship survivability requires abandoning the traditional zonal strategy prescribed by SOLAS (Lützen, 2001; Pawlowski, 2004) and using a direct non-zonal approach. This method allows deriving $p$ factors from an automatic generation of breaches from proper geometric and probabilistic models based on a Monte Carlo (MC) process. The evaluation of survivability follows the metrics derived by the residual stability of the ship.

The use of an MC approach is not new for ship survivability assessment in damage conditions, being widely applied not only for static analysis (Krüger et al., 2008; Krüger and Dankowski, 2019) but also for more advanced time-domain ship motions and flooding simulations (Vassalos, 2008; Spanos and Papanikolaou, 2014; Ruponen et al., 2019; Atzampos et al., 2019). However, MC sampling introduces

* Corresponding author.
*E-mail addresses:* francesco.mauro@strath.ac.uk (F. Mauro), d.vassalos@strath.ac.uk (D. Vassalos).

https://doi.org/10.1016/j.oceaneng.2022.111008
Received 9 November 2021; Received in revised form 7 February 2022; Accepted 28 February 2022
Available online 14 March 2022

randomness into the process, leading to a dispersion of obtained survivability indices within different batches of generated damages. A high number of samples (about 10,000) allows reducing this dispersion to acceptable levels, considering at least five calculation repetitions to obtain the final index (Bulian et al., 2016).

In the on-going EC project FLARE (2019-2022), one of the main goals is favouring direct approaches to determine the global risk of loss of lives for passenger ships after an accident (Vassalos, 2020). With ship survivability determination a significant step of the cumulative risk calculation process, improving the probabilistic framework for direct evaluation of ship survivability after damages is a logical step. A proper determination of ship survivability in a probabilistic framework requires the analysis of a high number of damage cases. Therefore, an attractive improvement in the present framework is the reduction of cases to be analysed, leading to a consequent reduction of computational effort, without losing accuracy on the final result. To this end, studies and applications in computer science suggest that Latin Hypercube (LH), Quasi-Monte Carlo (QMC) or Randomised Quasi-Monte Carlo (RQMC) methods ensure a faster convergence rate in evaluating complex functions (Cools and Nuyens, 2014). At present, concerning damaged ship survivability, a preliminary study, limited to bottom groundings, has been carried out for the non-zonal approach implementing a RQMC sampling method on a reference barge (Mauro et al., 2021).

The present work extends this preliminary research by implementing four different sampling procedures and comparing them for collisions, bottom and side grounding accidents. After an initial detailed analysis on a reference barge, the most promising procedure is compared with standard MC sampling on a passenger ship internal layout, highlighting the possibility of reducing the sample size to reach a specific confidence level for the survivability index.

## 2. Probabilistic framework for passenger ship survivability

According to the SOLAS2009 framework, the representative metric of the damaged ship survivability is the attained index of subdivision $A$. The scope of ship survivability assessment is to calculate a set of partial $A_i$ indices, compare them with a required subdivision index $R$ and ensure that $A_i \geq 0.9R$ for all the analysed conditions. This process applies not only to the traditional zonal approaches for collisions (SOLAS2009) but also to non-zonal ones (Bulian et al., 2019) (see Fig. 1), including also groundings/contacts. The generic and compact formulation for index $A$ adopted in this study is as follows:

$$A = \sum_{k=1}^{3} \sum_{j=1}^{N_d} w_{jk} A_{jk} \tag{1}$$

where $k$ denotes the damage type according to the following convention:

$k = 1$ : collisions (C00 damages);
$k = 2$ : bottom groundings (B00 damages);
$k = 3$ : side groundings/contacts (S00 damages).

Subscript $j$ indicates the $N_d$ calculation draughts for the index determination. The SOLAS framework prescribes the analysis of three draughts, namely:

$T_1$ : light service draught;
$T_2$ : partial subdivision draught;
$T_3$ : deepest subdivision draught.

Specific weights $w_{jk}$ apply to each combination of damage type and draught. Recent developments within FLARE projects suggests using only two draughts:

$T_{1_{FL}}$ : subdivision draught at $0.75(T_3 - T_1)$;

**Table 1**
Weighting factors $w_{jk}$ for $A$ index evaluation.

| | EMSA3 derived | | | FLARE (flooding) | | | |
|---|---|---|---|---|---|---|---|
| | | | | Cruise | | Ro-Pax | |
| | $T_3$ | $T_2$ | $T_1$ | $T_{1_{FL}}$ | $T_{2_{FL}}$ | $T_{1_{FL}}$ | $T_{2_{FL}}$ |
| *C*00 | 0.100 | 0.100 | 0.050 | 0.025 | 0.025 | 0.125 | 0.125 |
| *B*00 | 0.076 | 0.076 | 0.038 | 0.190 | 0.190 | 0.170 | 0.170 |
| *S*00 | 0.224 | 0.224 | 0.112 | 0.285 | 0.285 | 0.205 | 0.205 |

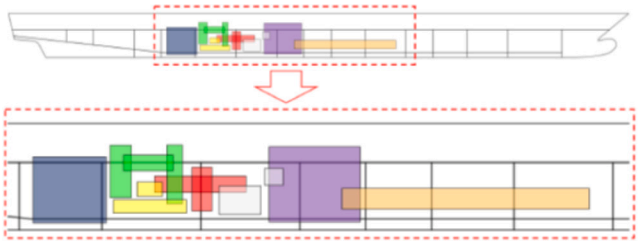

**Fig. 1.** Non-zonal approach representation (Bulian et al., 2019).

$T_{2_{FL}}$ : subdivision draught at $0.45(T_3 - T_1)$.

Dedicated analyses also provide specific weights for flooding casualties, considering a distinction between cruise ships and Ro-Pax vessels (Vassalos and Mujeeb-Ahmed, 2021). Table 1 reports the associated $w_{jk}$ according to EMSA3 (Bulian et al., 2019) and FLARE conventions.

Regardless of the metric adopted for the weighting factors, the partial $A_{jk}$ indices of Eq. (1) remain the same:

$$A_{jk} = \sum_{i=1}^{N_c} p_{ijk} s_{ijk} \tag{2}$$

where $i$ denote each of the $N_c$ unique groups of compartments describing a damage case, $p_{ijk}$ is the occurrence of each of the damage cases, and $s_{ijk}$ is linked to the probability to survive the flooding of the $i$-case damaged compartments. $s$ factors calculation is compliant with GZ-based methodology described by SOLAS2009. Of course, considering SOLAS2009 regulation, the value of $k$ in Eqs. (1) and (2) is restricted to 1.

However, the main difference between the zonal and non-zonal approaches resides in the prediction of the $p$ factors. SOLAS2009 determines $p$ through analytic formulation, reasonably applicable for C00 damages but not advisable for other damage types (Bulian and Francescutto, 2010). The adoption of a non-zonal approach implies the availability of a probabilistic model for damage dimensions and location. In such a way, the $p$ factors derive from a sufficiently large number of breaches generated by an MC sampling process. As the MC outcome is subject to uncertainties, the number of samples should be large enough to match the desired confidence level on the estimation of attained subdivision index.

A confidence interval $CI$ generally follows the Central Limit Theorem, and can be represented by a normal distribution. However, for small amount of repetitions $N_r$ (i.e. less than 30), the confidence interval $CI$ should be found using a Student distribution. Therefore, assuming the suggested number of $N_r$ is five, the following formulation for $CI$ is advisable for the partial indices of Eq. (2):

$$CI\,(c) = \overline{A_{jk}} \pm t \frac{\sigma}{\sqrt{N_r}} \tag{3}$$

where $c$ is the desired confidence level, $\overline{A_{jk}}$ is the mean value of $A_{jk}$, $t$ is the inverse cumulative density function of the Student $t$-distribution with confidence level $c$ and $N_r - 1$ degrees of freedom, while $\sigma$ is the

sample variance according to:

$$\sigma = \sqrt{\frac{1}{N_r - 1}\sum_{i=1}^{N_r}\left(A_{jk_i} - \overline{A_{jk}}\right)^2} \tag{4}$$

Extending $CI$ to the global attained index given in Eq. (1) is straightforward, as only sum and products between the partial indices should be performed.

The general logic of a non-zonal approach compliant with SOLAS2009 comprises the following:

1. Generation of sample breaches according to a probabilistic model of damage characteristics.
2. Determination of damage cases with associated $p$ factors.
3. Survivability assessment based on static stability calculations, determining $s$ factors.
4. Determination of $A$ index.

This approach is a simplified assessment of passenger ship survivability as it derives from static calculations. If more advanced time-domain simulations were used to determine the survivability (Vassalos, 2008; Spanos and Papanikolaou, 2014), the regrouping of breaches in damage cases is no longer possible and so is the use of $p$ factors. In such a case, a breach-by-breach analysis is necessary, increasing the total calculation time of the survivability assessment.

Further analysis on the sampling process, aimed to reduce the number of breaches or repetitions necessary to determine survivability, can improve the actual non-zonal approach probabilistic framework. The following sections discuss possible methods that could enhance the damage breaches sampling.

## 3. Damage breaches for ship survivability

The probabilistic assessment of ship damage survivability requires the definition of dedicated distributions to identify damage location and dimensions. The current probabilistic framework adopts a set of standard models describing those characteristics for different damage types based on accident database analyses, providing a clearly defined geometrical model for the considered breach.

### 3.1. C00 collision damages

Collisions are the standard damage type considered by SOLAS for the zonal approach; However, eSAFE and EMSA 3 project extends the non-zonal approach, originally developed for groundings, also to collision damages.

The non-zonal definition of a C00 damage follows the SOLAS zonal background (IMO, 2006), introducing the definition of the lower vertical limit of the breach (Bulian et al., 2019) to overcome the concept *worst case approach* intrinsic in SOLAS formulation. Therefore, the geometrical model of a non-zonal C00 model requires the description of the following characteristics:

- $X_M$ (m): longitudinal position of potential damage centre.
- $L_x$ (m): longitudinal extent of the potential damage.
- $L_y$ (m): lateral penetration of the potential damage.
- $z_{LL}$ (m): lower vertical limit of the potential damage.
- $L_z$ (m): vertical extension of the potential damage.
- $I_{side}$ (-): flag distinguishing starboard ($I_{side} = 1$) and portside ($I_{side} = -1$) damages.

Fig. 2 gives an overview of the geometrical model of a C00 collision, together with the independent marginal cumulative distributions of the mentioned breach characteristics in non-dimensional form. Starboard and portside damages are equiprobable. The damage is defined as *potential*, meaning that it could extend also outside the vessel limits. This aspect requires particular attention to the positioning of the damage at the ship extremities, keeping consistency with the analytical formulation of zonal $p$ factors. In case the potential damage is fully contained within the ship length $L_s$, $X_M$ corresponds to the damage centre. If the damage partially extends outside the vessel, then the location of $X_M$ should be changed as described by Bulian and Francescutto (2010).

Even though marginal distributions are supposed to be independent, attention should be paid to the damage penetration $L_y$. The SOLAS framework implicitly assumes that for a C00 damage the ratio between dimensionless penetration and dimensionless length cannot exceed 15. Therefore, an upper limit $L_{ymax} = 15(B/L_s)L_x$ should be introduced, having as main consequence that damage length should be generated before damage penetration. As a last remark, the internal limit of the damage follows the waterline at $z^* = T$ shifted by $L_y$, then the C00 damage is not always *box-shaped*.

### 3.2. B00 bottom grounding damages

B00 damages have a different definition compared to C00 collisions (Bulian et al., 2016). A B00 type damage is supposed to be *box-shaped* and has to be considered as a *potential*, meaning a damage that could extend also outside the vessel limits. Fig. 3 gives the geometrical description of the damage identifying main dimensions and locations, namely:

- $X_F$ (m): longitudinal position of potential damage forward end.
- $Y_F$ (m): lateral position of measured damage forward end centre.
- $L_x$ (m): longitudinal extent of the potential damage.
- $L_y$ (m): lateral extent of the potential damage.
- $L_z$ (m): vertical penetration of the potential damage.

Fig. 3 also shows the marginal cumulative distributions of the mentioned breach characteristics in non-dimensional form, as prescribed by the probabilistic framework for non-zonal approach. The geometric characteristics are independent variables, allowing a direct sampling of the given marginal distributions.

However, it is necessary to perform an additional step for the right lateral positioning of a B00 damage. $Y_F$ is not the lateral position of the potential damage box, but is the lateral position derived from a statistics of measurements on damaged ships. Therefore, defining $Y_{Fp}$, the lateral position of the potential damage centre, the following system needs to be solved for its evaluation:

$$\begin{cases} Y_{Fp} & = Y_F + \frac{\text{sign}(\delta)}{2}\max\left(L_y - L_{ylim}, 0\right) \\ \delta & = Y_F - \frac{y_1+y_2}{2} \\ L_{ylim} & = \min\left(2\left(y_1 - Y_F\right), 2\left(Y_F - y_2\right)\right) \end{cases} \tag{5}$$

where $y_1$ and $y_2$ are the portside and starboard side lateral coordinates of the reference waterline located at $z^* = z_{bottom} + L_z$ and x = $X_F$. For conventional ships $z_{bottom}$ is equal to zero. With the distribution of $Y_F$ given in the non-dimensional form $x_2$ (Fig. 3), the final lateral position of the potential damage forward end centre results in:

$$Y_{Fp} = \frac{y_1 + y_2}{2} + x_2 b_{(X_F, z^*)} \tag{6}$$

Therefore, the dimensional value $Y_{Fp}$ changes as a function of the longitudinal location $X_F$ and of the vertical penetration $L_z$.

### 3.3. S00 side grounding damages

The definition of a side grounding damage inherits some peculiarities from the previous two types of damages (Bulian et al., 2020). Also in this case, the damage is intended to be potential, thus extending outside the vessel. As for the C00 type damages, this damage may be either on starboard or on portside, with equal probability. Furthermore, the inner limit of the potential damage follows a specific waterline resulting in a non box-shaped damage. The modelling considers that the limiting waterline should be extended to the damage top $z^* = z_{LL} + L_z$.

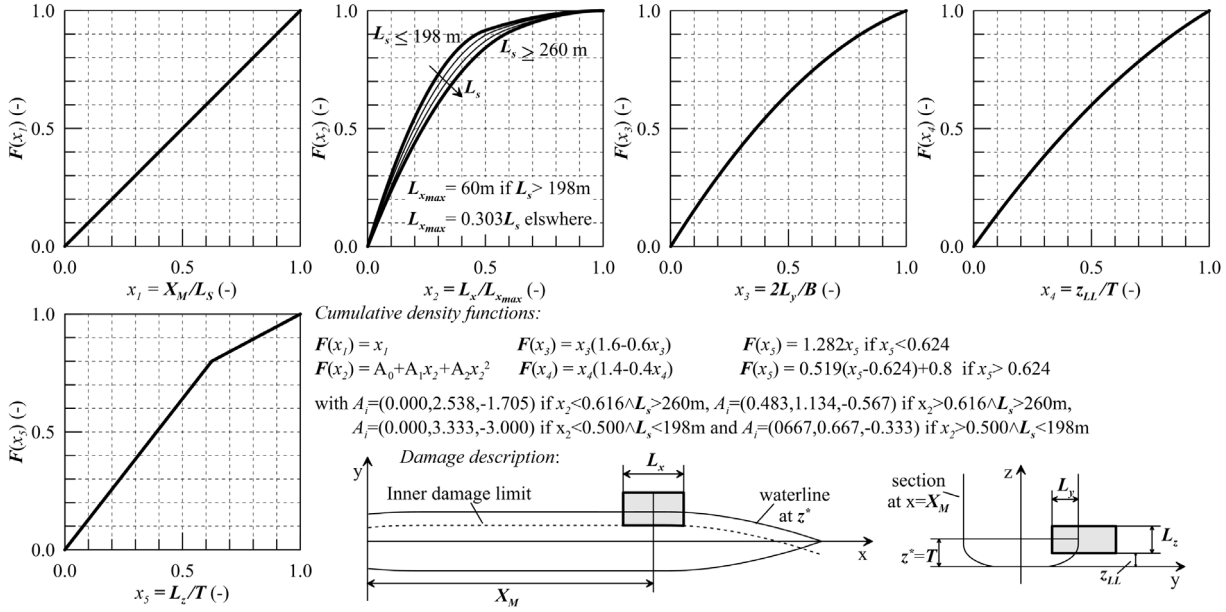


**Fig. 2.** Cumulative distributions of dimensionless characteristics and geometrical description of C00 collision damages.

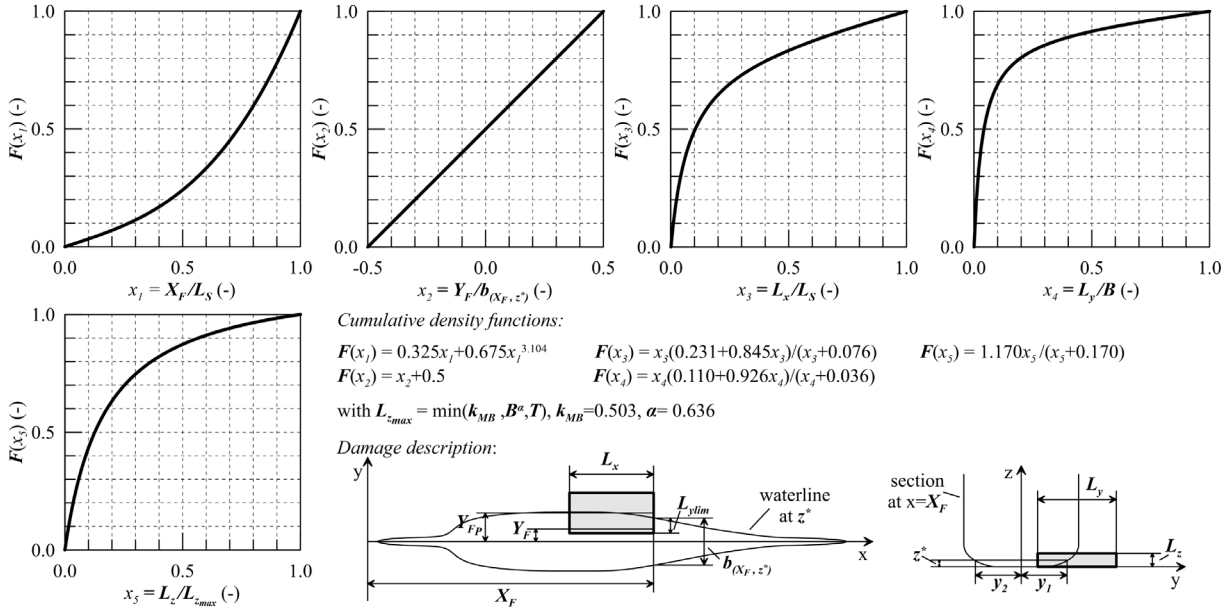


**Fig. 3.** Cumulative distributions of dimensionless characteristics and geometrical description of B00 bottom groundings damages.

However, the upper limitation can go above the ship geometry vertical limit (potential damage), therefore $z^*$ is always limited to the geometry top.

Fig. 4 shows the geometrical description of an S00 damage identifying main dimensions and locations with the associated marginal distributions:

- $X_F$ (m): longitudinal position of potential damage forward end.
- $L_x$ (m): longitudinal extent of the potential damage.
- $L_y$ (m): lateral penetration of the potential damage.
- $z_{LL}$ (m): lower vertical limit of the potential damage.
- $L_z$ (m): vertical extension of the potential damage.
- $I_{side}$ (-): flag distinguishing starboard ($I_{side} = 1$) and portside ($I_{side} = -1$) damages.

It can be observed that the longitudinal position of the forward end $X_F$ has the same non-dimensional distribution of B00 damages. However the final value is different as the limiting upper value is lower for S00 damages ($L_{xmax} < L_s$).

Fig. 4 reports also the marginal distribution of the damage breach characteristics. For the previous modellings, all the random variables are statistically independent. On the contrary S00 damage modelling assumes that $z_{LL}$ and $L_z$ are statistically dependent, but still independent from the remaining damage parameters. Therefore, the probabilistic modelling provides a joint distribution, derived by multiplying the marginal distribution of $z_{LL}$ and the conditional distribution of $L_z$. The damage height is conditioned to the occurrence of water ingress, which is embedded in the marginal distribution of $z_{LL}$ through the $z_{LLw}$ parameter.

As a result of this conditional modelling for the vertical location and dimension, a S00 damage is not necessary developing across the

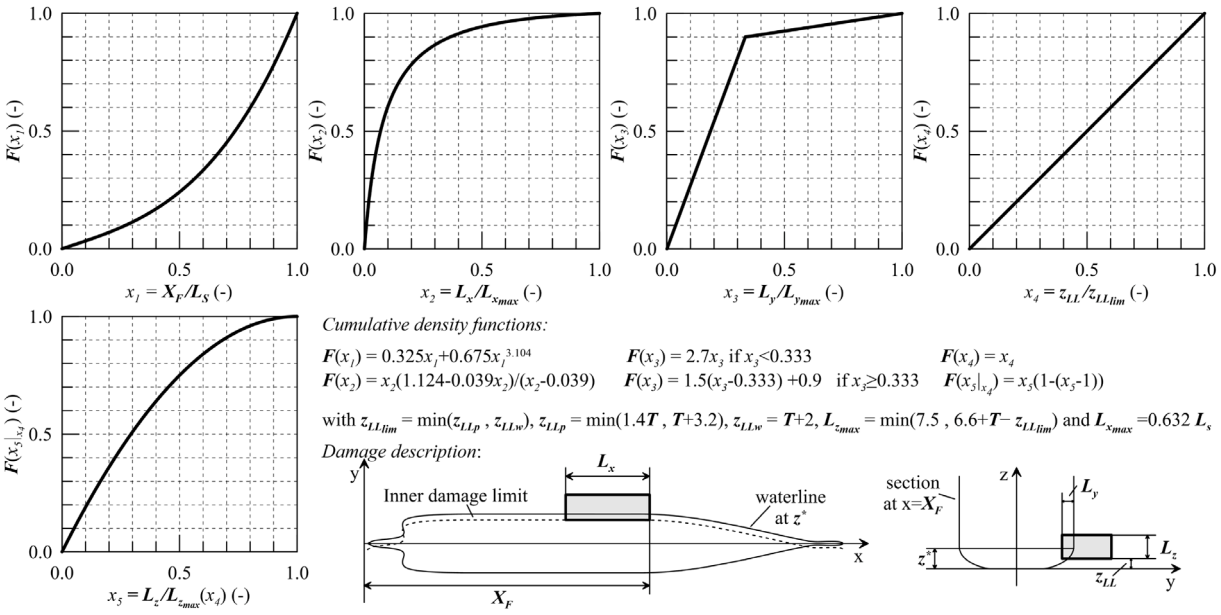


**Fig. 4.** Cumulative distributions of dimensionless characteristics and geometrical description of S00 side groundings damages.

design draught (as a C00 type) or only under it (as B00 damages). It is implied that for some cases an S00 damage can develop only above the considered draught.

## 4. Sampling strategies for MC integration

The direct non-zonal approach for passenger ship survivability described in Section 2 allows the application of non deterministic MC-like integration to determine the attained survivability index. The strategy is applicable for the global index of Eq. (1) and the partial indices of Eq. (2). In particular, Eq. (2) is already representative of a multidimensional MC integration process having the following form for the integral value:

$$I = \int_{\Omega} f(\mathbf{x})\,\mathrm{d}\mathbf{x} \approx \frac{1}{N_s}\int_{\Omega}\mathrm{d}\mathbf{x}\sum_{i=0}^{N_s-1} f(\mathbf{x}_i) \tag{7}$$

where $\Omega \subset \mathbb{R}^m$ is a probability space having $m$ dimensions, $\mathbf{x} = (x_1, \ldots, x_m) \in \Omega$ is a set of independent random variables and $N_s$ is the number of samples. In case $\Omega = (0,1)^m$ (unit hypercube), then $\int_{\Omega}\mathrm{d}\mathbf{x} = 1$ and $\mathbf{x}$ is described by uniform random variables $\mathbf{U} \sim \mathcal{U}(0,1)^m$. Therefore, Eq. (7) becomes:

$$I \approx \hat{I}_n = \frac{1}{N_s}\sum_{i=0}^{N_s-1} f(\mathbf{U}_i) \tag{8}$$

Rewriting Eq. (2) in the form of Eq. (8) leads to the following formula:

$$A_{jk} \approx \sum_{i=1}^{N_c}\frac{n_i(\mathbf{U})}{N_s}s_{ijk} = \sum_{i=1}^{N_c} p_{ijk}(\mathbf{U})\,s_{ijk} \tag{9}$$

where $n_i$ are the number of breaches comprising one damage case, which is a function of the uniform random variables $\mathbf{U}$. It is evident from Eq. (9) that the $p$-factors are direct functions of the random variables required by the MC process. Therefore, the method adopted to generate the uniform random variables $\mathbf{U}$, governing the integration process, influences the stochastic variability of the integral upon consecutive repetitions. Direct sampling of $\mathbf{U}$ through pseudo-random numbers represents the standard *crude MC method* (Hammersley and Handscomb, 1964). According to the strong law of large numbers, the approximated integral always converges to the exact value as $N_s$ increases without bounds.

Performing an excessively high number of samples is not convenient; therefore, the estimate is subject to an error. Supposing that $f$ has finite variance defined as:

$$\sigma^2 = \int_{\Omega}(f(\mathbf{x}) - I)^2\,\mathrm{d}\mathbf{x} \tag{10}$$

It follows that $E((\hat{I}_n - I)^2) = \sigma^2/N_s$ and, consequently, the root mean square error of an MC sampling is in the order $O(1/\sqrt{N_s})$. Such a rate is an improvement compared to classical quadrature rules for multidimensional problems and discontinuous functions; however, alternative approaches may further reduce the variance of the process.

The following sections describe possible upgrades that can reduce the standard deviation of the MC process by changing the sampling technique.

### 4.1. Latin hypercube approach

An alternative solution for sampling uniform distribution to reduce the variance of MC integral is stratification. This technique divides the domain $\Omega$ into distinct adjacent strata $\Delta\omega_i$ and estimates the integral by combining sub-values obtained in the single strata.

Simple stratification with a proportional allocation of samples in the strata generates the same variance of the MC approach. However, considering multidimensional problems, stratification should be performed through all the $m$ dimensions, adopting the so-called Latin Hypercube sampling (McKay et al., 1979). The generation of LH implies using random permutations, which means that all the possible $N_s$ ordering of $\mathbf{x}_i$ are equiprobable. Random permutation changes the array's elements, swapping the $i$th element of the original array with the $k$th one, assuming that $k$ is a randomly distributed number in $[0, N_s - 1]$.

It has been demonstrated (Owen, 1997) that the variance of an integral estimate using LH sampling with $N_s \geq 2$ is as follows:

$$\mathrm{Var}\left(\hat{I}_{n_{LH}}\right) = E\left(\left(\hat{I}_{n_{LH}} - I\right)^2\right) \leq \frac{\sigma^2}{N_s - 1} \tag{11}$$

Therefore, the order of convergence of LH sampling is always lower than the crude MC sampling.

### 4.2. Quasi-random approach

An alternative to LH sampling is the adoption of the so-called quasi-random methods (Niederreiter, 1987). The idea is to completely

abandon the randomness of the sampling process, distributing samples locations uniformly as possible in a deterministic way.

It is possible to evaluate an estimator for the irregularity of the sample spatial distribution and try to minimise it. A typical irregularity measure is the *star discrepancy*. Considering a set of points $\mathbf{P} = \{p_1 \cdots, p_{N_s}\}$ in a unit hypercube $\Omega = (0,1)^m$, $\Omega$ can be described by a set of $m$ axis-aligned boxes $B_i$ having one corner in the origin, ideally containing the same number of samples $N_{B_i} = N_s/m$ or, more generally, $N_{B_i} = N_s\lambda(B_i)$, where $\lambda(B_i)$ is the volume of $B_i$. Then, star discrepancy measures for $\mathbf{P}$ the distance between real and ideal situations:

$$D^*_{N_s}(\mathbf{P}) = \sup_{B\subset\Omega}^{*} \left| \frac{N^*_{B_i}}{N_s} - \lambda(B_i) \right| \tag{12}$$

where $N^*_{B_i}$ is the real number of points in each box $B_i$. The discrepancy is related to the integration error. Therefore, the adoption of samples with low $D^*$ reduces the variance of the process. Low-discrepancy sequences (LDS) of points reduce $D^*$ to a level that allows obtaining in the worse case an error $O((\log N_s)^m/\sqrt{N_s})$ for an MC integration process. However, practical application problems shows that the use of quasi-random sequences is always giving lower errors than crude MC (Niederreiter, 1992).

#### 4.2.1. Sobol sequences

Different methods can be used to generate deterministic LDS, as the Halton, Faure, Sobol or Niederreiter ones (Niederreiter, 1988). Sobol sequences is an attractive method, as several studies have proven its advantages compared to other LDSs (L'Ecuyer and Lemieux, 2002; Jaeckel, 2002). This is true because the sequence has been constructed such as to have a better uniformity of distribution with increasing sample but a good distribution even with fairly small initial samples with a very fast computational time (Sobol et al., 2011).

The generation of a Sobol sequence starts from the selection of a set of polynomials of $n_j$ degree $P_j = x^{n_j} + a_{1,j}x^{n_j-1} + a_{2,j}x^{n_j-2} + \cdots + a_{n_j-1,j}x + 1$, where coefficients $a_{i,j}$ are either 0 or 1, are used to generate a sequence of positive integer numbers according to the following recursive relation:

$$m_{k,j} = 2a_{1,j}m_{k-1,j} \oplus 2^2 a_{2,j}m_{k-2,j} \oplus \cdots \oplus 2^{n_j} m_{k-n_j,j} \oplus m_{k-n_j,j} \tag{13}$$

where $\oplus$ is the bit-by-bit exclusive-or operator, $1 \le k \le n_j$ is odd and $n_j \le 2^k$. Finally, the $j$th component of the $i$th point of the Sobol sequence is given by:

$$x_{i,j} = i_1 v_{1,j} \oplus i_2 v_{2,j} \oplus \cdots \tag{14}$$

where $v_{i,j} = m_{i,j}/2^k$ and $i_k$ is the $k$th binary digit of $i$. The process can be implemented in software programs, generating Sobol sequences with low computational effort (Levitan et al., 1988; Bradley and Fox, 1988).

#### 4.2.2. Randomised LDS

The adoption of LDS does not allow obtaining a sample-based error estimate, with the sequence being the same at each sample. An RQMC (Randomised Qasi-Monte Carlo) method permits to re-randomise an LDS sequence, transforming a QMC (Quasi-Monte Carlo) sequence $p_i$ into random points $x_i$ that retain QMC properties and expectation of $I$.

The simplest way to achieve this property is to consider $x_i = (0,1)^m$ and repeat $N_r$ times independent QMC integrations giving a combined estimate $\hat{I} = 1/N_r \sum_{i=1}^{N_r} \hat{I}_r$ with expected value $I$. The $x_i$ sequence may originate from modulo rotation methods on integration lattices (Cranley and Patterson, 1976) or digital nets (Tuffin, 1996). Alternatively, $x_i$ may derive from a scrambling process applied to the original sequence (Owen, 1997).

General uniformly distributed permutations of base $b$ digits of a sequence allow maintaining all the properties of the original $p_i$. However, this scrambling process requires a large number of permutations. More convenient is the usage of random linear scrambling (Matušek, 1998). As the final RQMC sequence maintains a QMC structure, the theoretical order of convergence for the integral should be $O((\log N_s)^m/N_s)$ or $O((\log N_s)^{(m-1)/2}/N_s^{3/2})$ in case of smooth functions.

### 4.3. Developed sampling methods

The effectiveness of the sampling method described in the previous sections cannot be determined a priori, as the general indication on the order of error represents just theoretic upper limits.

An effective determination of the most suitable method for a given problem necessitates a testing and comparison of a set of methods, assessing the best option for the specific case. In this study, aiming to find a sampling procedure to reduce data dispersion for the survivability index of a damaged ship, the following sampling strategies have been implemented:

**SMPL-0** Crude MC sampling.

**SMPL-1** LH sampling.

**SMPL-2** RQMC method based on mono-dimensional Sobol sequences.

**SMPL-3** RQMC method based on a multidimensional Sobol sequence.

The first method (*SMPL-0*) represents the standard methodology currently used to sample damages in a non-zonal damage stability framework (Bulian et al., 2020) and is here used as a reference for the other procedures. *SMPL-1* represents a first possibility of variance reduction, implementing the LH method described in the previous section. *SMPL-2* and *SMPL-3* are both RQMC methods based on Sobol sequences. However, in method *SMPL-2* a diverse sequence is generated for each sampled variable, with a dedicated scramble process per each sequence. In *SMPL-3*, only a QMC sequence is generated with a single multidimensional scrambling process.

The described sampling processes differs from the ways used to generate uniform distributions of numbers. It is then useful to observe the differences between uniform distributions resulting from the four methods. Fig. 5 shows the comparison of the proposed methods using different sample sizes. It is evident that increasing the sample size, all methods are capable to accurately reproduce $\mathbf{U}^1$, However, decreasing the samples number, the accuracy of fitting $\mathbf{U}^1$ with *SMPL-0* decreases. All the other methods have a good accuracy also with relatively few samples. In particular, *SMPL-1* is always capable to reproduce a marginal uniform distribution because of the stratified nature of the method. It should be noted, that *SMPL-2* and *SMPL-3* are equivalent for the mono-dimensional case, the small differences referring only to the random seed of the scrambling process on the QMC sequence.

However, the probabilistic description of ship damages requires the sampling of multidimensional variables. Therefore, Fig. 6 shows an example of a bi-dimensional uniform distribution. This example helps to understand the coverage of the potential sampling space granted by the different procedures. It results that *SMPL-0*, *SMPL-1* and *SMPL-2* are affected by data agglomerations, also with a number of samples suitable to reproduce the marginal uniform distribution. This is true also for *SMPL-2* based on mono-dimensional QMC sequences. In fact, the coupling between different dimensions is no longer ruled by a QMC sequence, resulting in a comparable coverage as granted by crude MC and LH approaches. On the contrary, the RQMC process implemented with *SMPL-3* maintains the QMC low discrepancies characteristics also in a multidimensional sampling. The example in Fig. 6 confirms the capability of *SMPL-3* to avoid sample agglomerations, ensuring the low discrepancy of the QMC sampling, regardless the random scrambling procedure embedded in the process.

The proposed simple example shows that it is not sufficient to implement a method capable to well reproduce a marginal uniform distribution, without ensuring low discrepancy in multidimensional cases. Methods based on LH have a pure random coupling between dimensions, the same for the RQMS method based on mono-dimensional sequences. Multidimensional low discrepancy can be granted by methods like *SMPL-3*. For such a reason, it could be expected that the

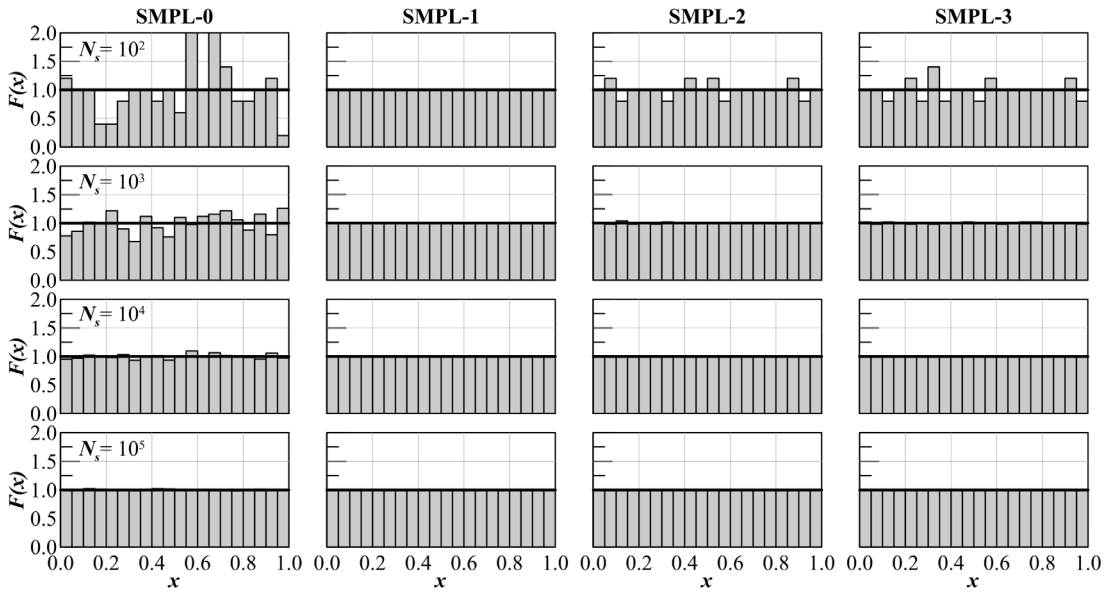


**Fig. 5.** Uniform distribution according to different sampling methods and sample size.

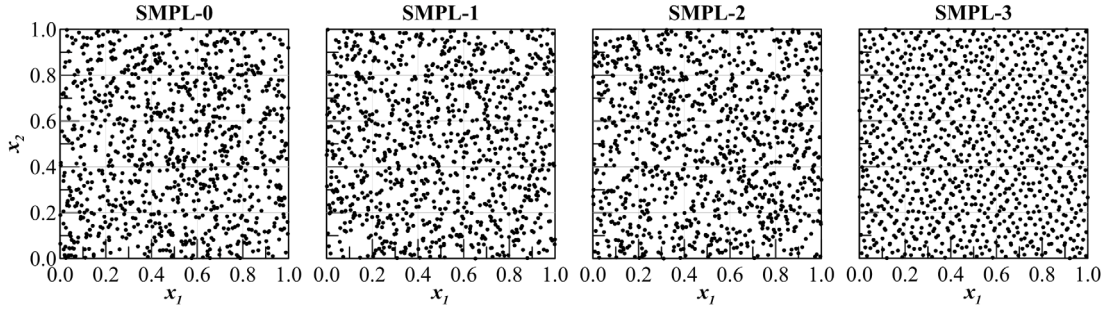


**Fig. 6.** Bi-dimensional distribution according to different sampling methods considering a sample size of $10^3$.

consequent variance reduction associated to the sampling method could be higher in *SMPL-3* than in *SMPL-2*, *SMPL-1* and *SMPL-0*, as the process is less subject to randomisation effects.

For the specific case of ship damages, from Eq. (9) it results that $p$-factors are a function of the uniform random variables $\mathbf{U}$. More precisely, the connection between $\mathbf{U}$ and the final factor is given by the probabilistic definition of the damage characteristics. Therefore, the sampling process for ship damages should be adapted to non-uniform distributions.

#### 4.3.1. Sampling non-uniform distributions

There are several ways that could be pursued to sample independent random variables according to a defined non-uniform distribution starting from sampling uniform distributions. The most commonly adopted, and used in this work, is based on the inversion of a given cumulative density function $F(x)$ and can be applied regardless of the method used to generate uniformly distributed numbers.

The sampling is based upon the following general property; if $F$ is a continuous cumulative density function in $(-\infty, +\infty)$ with inverse $F^{-1}$ defined by:

$$F^{-1}(u) = \inf\{x : F(x) = u, 0 \le u \le 1\} \tag{15}$$

If $\mathbf{U}$ is a uniform random variable in $[0, 1]$, then $F^{-1}(\mathbf{U})$ is distributed according to $F$, and also if a variable $X$ has cumulative $F$ (and associated density $f$), then $F(\mathbf{X})$ is uniformly distributed in $[0, 1]$. The property is also extended to distributions with finite support as is the case for damage breach characteristics. Fig. 7 shows the inversion process for general theoretical continuous distributions. In general, the procedure for a generic array of random variables $\mathbf{X}$ can be summarised in the following steps, assuming we know the starting $f(\mathbf{X})$ for the final sample:

1. Compute the cumulative density function $F(\mathbf{X})$.
2. Compute the inverse $F^{-1}(\mathbf{X})$.
3. Sample $\mathbf{U}$ $(0, 1)$.
4. Compute $F^{-1}(\mathbf{U})$.

The described procedures can easily be applied to the probabilistic description of C00, B00 and S00 damage characteristics presented in Section 2.

## 5. Survivability assessment on a reference barge

The proposed sampling procedure is here applied to a reproducible barge available in literature for bottom groundings damage survivability (Bulian et al., 2016). This barge has been used because it represents a good benchmarking example for damage stability assessment. Therefore, it is the most indicative case for testing new procedures/methods for damage stability calculations.

The main characteristics of the barge are summarised in Table 2, and a view of the general arrangement is given in Fig. 8. The internal subdivision is quite simple, being composed only by box-shaped compartments. A double bottom is present with a height of 1.6 m, divided in 10 longitudinal zones, and, except for the fore and aft end, in 3 transversal zones. The double bottom compartments are associated with an unprotected opening (represented as black squares in Fig. 8),

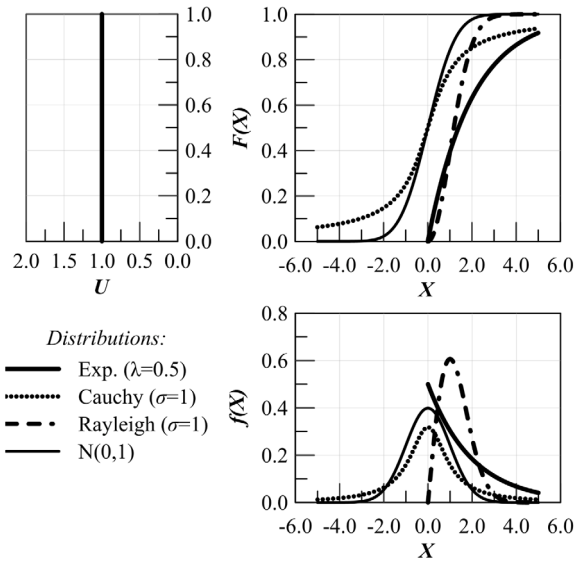


**Fig. 7.** Inversion method example for general theoretical continuous statistical distributions.

**Table 2**
Test barge main characteristics.

| Quantity | | Value | Unit |
|---|---|---|---|
| Length over all | $L_{OA}$ | 100.0 | m |
| Breadth | $B$ | 16.0 | m |
| Construction height | $D$ | 10.0 | m |
| Lower subdivision draught | $T_1$ | 3.0 | m |
| Partial subdivision draught | $T_2$ | 3.6 | m |
| Deepest subdivision draught | $T_3$ | 4.0 | m |
| Metacentric height | $GM_T$ | 2.0 | m |

vertically positioned at 7.5 m above the ship bottom and longitudinally positioned at the compartment centre. For the central compartments, the opening is transversally centred, while the side one is located at 7.5 m from centreline to starboard or portside. The internal layout consists then in a total of 37 rooms, more specifically 26 in the double bottom, 10 in the lower deck and 1 in the upper deck. The permeability $\mu$ of the spaces is constant and equal to 1.00. All the tested droughts have a $GM_T$ of 2.0 m, following the simplified assumptions of the pilot studies on this reference barge.

The following sections give an overview of the calculations performed and the results obtained on this reference geometry, sampling the C00, B00 and S00 type damages with the four different procedures described in Section 3. The static calculations for the damage cases have been performed with the static calculation routines of software PROTEUS3 (Jasionowski, 2001) available at MSRC.

### 5.1. A-index evaluation

The calculation of A-index follows SOLAS2009 regulations for passenger ships, considering only the final stage of flooding. However, the simplified internal layout of the test barge makes the analysis of intermediate flooding stages unnecessary, as there are not restricted spaces limiting the flooding process that may justify a non-instantaneous flooding of the rooms.

External moments are neglected for B00 and S00 damage type to ensure compliance with simulations performed by Bulian et al. (2020) on the same test case. Simulations for C00 damage types consider external loads due to passengers on side, considering 750 passenger of 75 kg each positioned at 7.2 m from centreline (Bulian et al., 2016). At the first instance, the safety metrics derived from eSAFE and EMSA3 project (see Table 1) have been used to weight the relative $A_{jk}$ for the total $A$-index determination. The estimation of $s$ factors follows the SOLAS prescriptions for passenger ships, without taking into account the fact that the upper deck could be associated with an open car deck of a Ro-Pax vessel.

Different sets of calculations have been carried out to study the variability of the sampling process on the barge survivability. Three increasing sample sizes have been considered to evaluate the influence of $N_s$ on the variance of the MC process (see Eq. (9)), more precisely: $10^3$, $10^4$ and $10^5$. To take into account the effect of the sample-based error estimate, 20 repetitions have been carried out for all the sample sizes, estimating all the times $A_{jk}$. This calculation scheme has been followed for the four sampling procedures described in Section 3.

The variability on the $A$-index is measured considering the 95% confidence interval on the mean value, calculated according to Eq. (3). Being $N_r$ equal to 20, the corresponding value for the inverse cumulative density function $t$ is 1.729.

Table 3 presents $A_{jk}$ mean values and the 95% confidence interval on the mean resulting from the 20 repetitions for all the four sampling procedures. The obtained values for the conventional crude MC method *SMPL-0*, shows that the obtained values for B00 and S00 damage types are in line with a previous pilot study on the same test case (Bulian et al., 2020), giving sufficient confidence to the reliability of the presented data.

Analysing the results, it appears that the mean values $\overline{A_{jk}}$ of the partial indices is not strongly influenced by either the $N_s$ and the sampling process. Considering C00 damage types, the variations between values at same $T$ and different $N_s$ are between 0.3 and 0.6% for all the implemented sampling methods. B00 and S00 damage types have sensible lower variations compared to C00 types, having a maximum difference around 0.3%, regardless the sampling method. Therefore, considering 20 repetitions, the mean value of the relative $A_{jk}$ can be considered, for the analysed case, independent from sample size and sampling method. The same cannot be stated for the confidence interval $CI$ on the mean.

Having a look to all the three draughts, the $CI$ has the same order of magnitude within the same sampling methods and size. However, the $CI$ varies across the sampling size and methods. For all the four sampling methods, an increase of sample size $N_s$ decreases the $CI$. All damage types show this trend, with C00 damages having $CI$ generally higher than S00 damages. B00 damages shows the lowest $CI$ in almost all the conditions tested.

Going deeper in the analysis, it can be observed that the $CI$ between different sampling procedures changes by keeping $N_s$ constant. For $N_s = 10^3$ *SMPL-0* has the highest $CI$ values for all the damage types, *SMPL-1* and *SMPL-2* have comparable $CI$ levels that are in any case from 20% up to 54% less than *SMPL-0* values. *SMPL-3* grants the best $CI$ reduction from conventional crude MC method, namely up to 73% for C00, 69% for B00 and 66% for S00 damages, with small variations among the different draughts. Increasing $N_s$ to $10^4$, the trend between the sampling procedures remains the same, with *SMPL-0* having the higher $CI$ and *SMPL-1* and *SMPL-2* showing comparable $CI$ reduction of the same magnitude of the $N_s = 10^3$ cases. *SMPL-3* remains the sampling method with highest $CI$ reduction capability; however, the reduction magnitude increases compared to the lower sample size. In this case, the $CI$ is up to 77% lower for C00, 86% for B00 and 85% for S00 damage types. Also in this case there are small variations within the three loading conditions. It is interesting to point out that, for the tested geometry, the $CI$ given by *SMPL-3* with $N_s = 10^3$ is comparable to the one given by the standard *SMPL-0* with $N_s = 10^4$. Finally, with $N_s = 10^5$, the $CI$ reduction from *SMPL-0* to *SMPL-3* becomes 82% for C00, 89% for B00 and 82% for S00 damage types. Also for this high $N_s$ the behaviour of *SMPL-1* and *SMPL-2* is equivalent to the previously mentioned cases.

All these considerations can be easily visualised in Fig. 9, where the values of the 20 repetitions are represented as a function of the sampling size $N_s$. To limit the amount of sub-figures, Fig. 9 represents

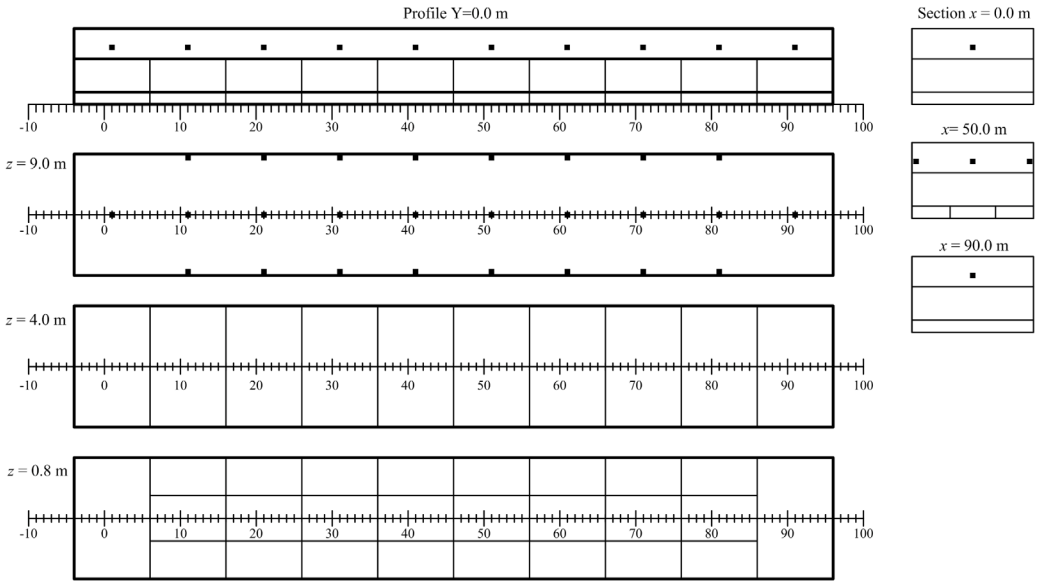


**Fig. 8.** Test barge general layout and openings.

**Table 3**
$A_{jk}$ values for the test barge case.

| | | SMPL-0 | | | SMPL-1 | | | SMPL-2 | | | SMPL-3 | | |
|---|---|---|---|---|---|---|---|---|---|---|---|---|---|
| | | $T_1$ | $T_2$ | $T_3$ | $T_1$ | $T_2$ | $T_3$ | $T_1$ | $T_2$ | $T_3$ | $T_1$ | $T_2$ | $T_3$ |
| | | $N_s = 10^3$ | | | | | | | | | | | |
| C00 | $\overline{A_{jk}}$ | 0.7906 | 0.7784 | 0.7095 | 0.7951 | 0.7789 | 0.7119 | 0.7932 | 0.7783 | 0.7132 | 0.7948 | 0.7775 | 0.7169 |
| | $CI(95\%)$ | ±4.54E−3 | ±5.75E−3 | ±7.06E−3 | ±3.58E−3 | ±2.78E−3 | ±3.52E−3 | ±2.62E−3 | ±2.98E−3 | ±3.94E−3 | ±1.96E−3 | ±2.90E−3 | ±1.91E−3 |
| B00 | $\overline{A_{jk}}$ | 0.8983 | 0.9228 | 0.9261 | 0.8975 | 0.9254 | 0.9238 | 0.8987 | 0.9243 | 0.9227 | 0.8971 | 0.9236 | 0.9230 |
| | $CI(95\%)$ | ±2.39E−3 | ±2.18E−3 | ±2.56E−3 | ±2.16E−3 | ±2.07E−3 | ±1.49E−3 | ±2.19E−3 | ±1.66E−3 | ±1.71E−3 | ±1.06E−3 | ±6.77E−4 | ±8.13E−4 |
| S00 | $\overline{A_{jk}}$ | 0.8793 | 0.9054 | 0.8549 | 0.8784 | 0.9045 | 0.8536 | 0.8787 | 0.9052 | 0.8522 | 0.8782 | 0.9031 | 0.8531 |
| | $CI(95\%)$ | ±3.48E−3 | ±3.49E−3 | ±4.54E−3 | ±1.63E−3 | ±2.71E−3 | ±2.51E−3 | ±1.52E−3 | ±2.25E−3 | ±4.01E−3 | ±1.18E−3 | ±1.39E−3 | ±2.19E−3 |
| | | $N_s = 10^4$ | | | | | | | | | | | |
| C00 | $\overline{A_{jk}}$ | 0.7935 | 0.7808 | 0.7132 | 0.7927 | 0.7766 | 0.7121 | 0.7927 | 0.7775 | 0.7124 | 0.7929 | 0.7775 | 0.7125 |
| | $CI(95\%)$ | ±1.20E−3 | ±1.97E−3 | ±1.48E−3 | ±1.05E−3 | ±8.69E−4 | ±9.58E−4 | ±8.08E−4 | ±1.21E−3 | ±1.07E−3 | ±4.29E−4 | ±7.19E−4 | ±3.87E−4 |
| B00 | $\overline{A_{jk}}$ | 0.8985 | 0.9235 | 0.9239 | 0.8972 | 0.9236 | 0.9245 | 0.8973 | 0.9241 | 0.9238 | 0.8975 | 0.9238 | 0.9239 |
| | $CI(95\%)$ | ±1.05E−3 | ±8.99E−4 | ±9.59E−4 | ±6.60E−4 | ±5.08E−4 | ±4.56E−4 | ±6.47E−4 | ±6.69E−4 | ±4.54E−4 | ±1.51E−4 | ±1.67E−4 | ±1.57E−4 |
| S00 | $\overline{A_{jk}}$ | 0.8798 | 0.9045 | 0.8511 | 0.8788 | 0.9046 | 0.8520 | 0.8792 | 0.9035 | 0.8518 | 0.8790 | 0.9036 | 0.8524 |
| | $CI(95\%)$ | ±1.51E−3 | ±9.92E−4 | ±1.47E−3 | ±7.88E−4 | ±6.74E−4 | ±8.50E−4 | ±7.77E−4 | ±6.02E−4 | ±9.58E−4 | ±2.34E−4 | ±2.53E−4 | ±4.39E−4 |
| | | $N_s = 10^5$ | | | | | | | | | | | |
| C00 | $\overline{A_{jk}}$ | 0.7929 | 0.7778 | 0.7125 | 0.7934 | 0.7781 | 0.7124 | 0.7934 | 0.7786 | 0.7119 | 0.7931 | 0.7781 | 0.7123 |
| | $CI(95\%)$ | ±4.89E−4 | ±5.62E−4 | ±6.17E−4 | ±5.34E−4 | ±6.46E−4 | ±3.96E−4 | ±3.49E−4 | ±2.72E−4 | ±3.59E−4 | ±8.78E−5 | ±1.41E−4 | ±1.07E−4 |
| B00 | $\overline{A_{jk}}$ | 0.8979 | 0.9238 | 0.9238 | 0.8977 | 0.9238 | 0.9237 | 0.8977 | 0.9239 | 0.9237 | 0.8976 | 0.9238 | 0.9238 |
| | $CI(95\%)$ | ±2.96E−4 | ±1.74E−4 | ±3.20E−4 | ±2.38E−4 | ±1.80E−4 | ±1.79E−4 | ±1.91E−4 | ±1.45E−4 | ±2.27E−4 | ±4.10E−5 | ±3.52E−5 | ±3.36E−5 |
| S00 | $\overline{A_{jk}}$ | 0.8787 | 0.9035 | 0.8524 | 0.8789 | 0.9040 | 0.8522 | 0.8788 | 0.9038 | 0.8523 | 0.8789 | 0.9038 | 0.8521 |
| | $CI(95\%)$ | ±3.05E−4 | ±3.19E−4 | ±4.30E−4 | ±2.38E−4 | ±2.74E−4 | ±3.01E−4 | ±2.27E−4 | ±1.98E−4 | ±3.72E−4 | ±5.50E−5 | ±4.74E−5 | ±1.08E−4 |

$A_k$ indices instead of $A_{jk}$ ones, together with the global $A$. $A_k$ values are a partial sum of the $A_{jk}$ grouping all the draughts of the same damage type as follows:

$$A_k = \sum_{j=1}^{3} w_{jk} A_{jk} \tag{16}$$

where $k$ denotes C00 ($k = 1$), B00 ($k = 2$) and S00 ($k = 3$) damage types, and the relative weights $w_{jk}$ are the one reported in Table 1 for the EMSA3 case. Fig. 9 reports also the mean value $\overline{A}$ within an interval $2\sigma$ evaluated according to Eq. (4). It has been selected to plot $\sigma$ instead of $CI$ for clarity of visualisation in the graph. With all the cases evaluated with the same $t$ and $N_r$, the trend identified by $\sigma$ is equal to the one given by $CI$.

The weights $w_{jk}$ modify the importance of single draughts and damage types in the determination of the final $A$-index. Therefore, it is necessary to analyse the results obtained for $A$. Fig. 9 reports in the final row the total $A$-index results (Eq. (1)) considering the EMSA3 metrics. From a visual screening it appears that the considerations deducted for the relative $A_{jk}$ are valid also for $A$. A proof is given by $\overline{A}$ and 95% $CI$ values reported in Table 4.

As mentioned, the final $A$ values derives from the metrics used to combine $A_{jk}$ coefficients for specific loading conditions. Therefore, it is useful to verify whether the adoption of different safety metrics influences the $CI$ values of the analysed sampling procedures. To this end, an additional set of calculations has been carried out to evaluate the metrics suggested in FLARE project (see Table 1). With the FLARE approach based on different loading conditions than the SOLAS ones,

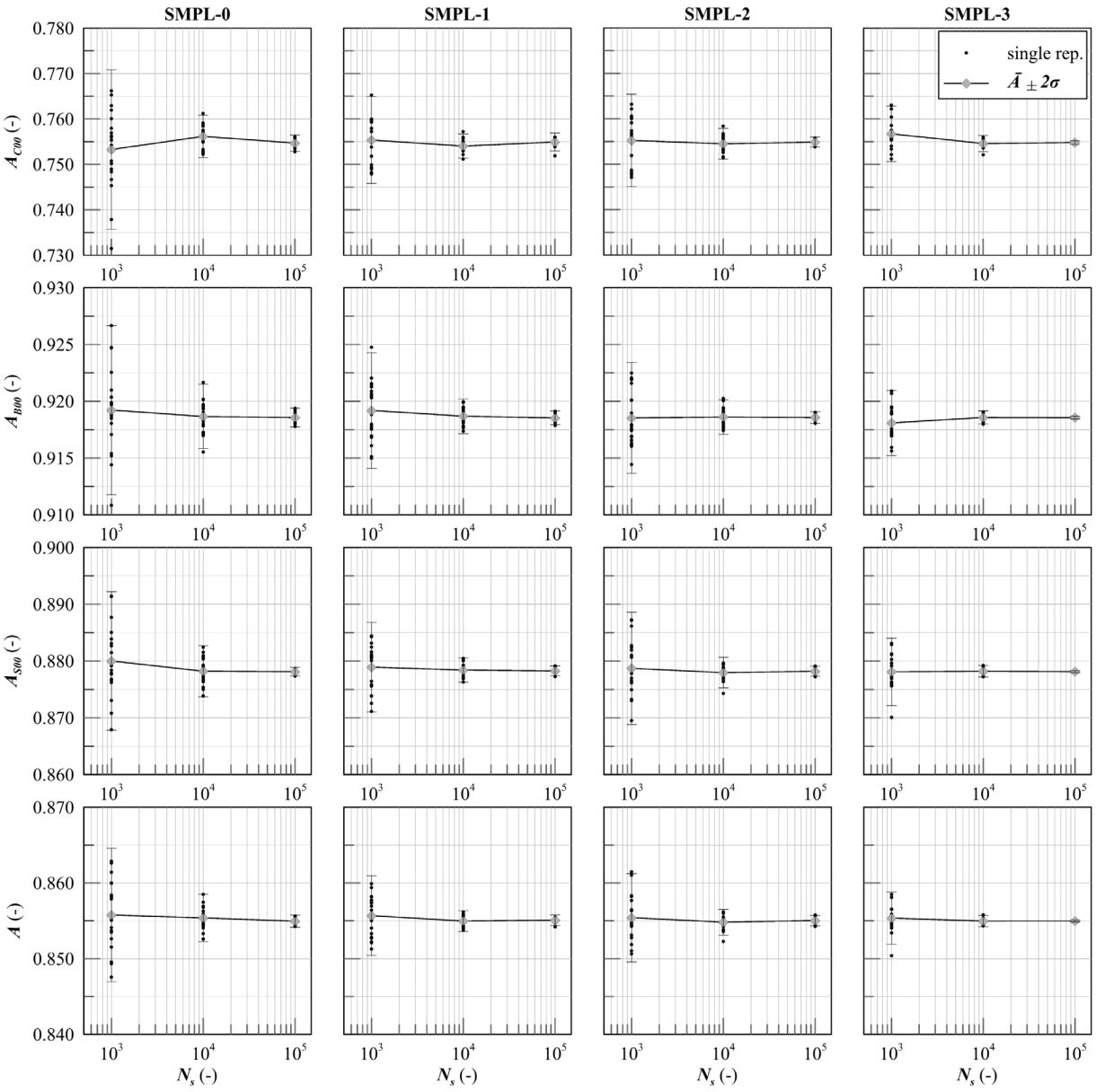


**Fig. 9.** Damage type specific and global attained index calculations on the test barge using the implemented sampling processes.

**Table 4**
$A$ mean values and 95% confidence interval for the barge case according to EMSA3 and FLARE safety metrics.

| SMPL | | $N_s = 10^3$ | | $N_s = 10^4$ | | $N_s = 10^5$ | |
|---|---|---|---|---|---|---|---|
| | | *EMSA3* | *FLARE* | *EMSA3* | *FLARE* | *EMSA3* | *FLARE* |
| 0 | $\bar{A}$ | 0.8558 | 0.8930 | 0.8554 | 0.8926 | 0.8549 | 0.8926 |
| | $CI$ | ±1.71E−3 | ±1.77E−3 | ±6.06E−4 | ±4.68E−4 | ±1.57E−4 | ±2.09E−4 |
| 1 | $\bar{A}$ | 0.8557 | 0.8915 | 0.8550 | 0.8929 | 0.8551 | 0.8925 |
| | $CI$ | ±1.01E−3 | ±1.32E−3 | ±2.67E−4 | ±3.71E−4 | ±1.35E−4 | ±1.26E−4 |
| 2 | $\bar{A}$ | 0.8554 | 0.8925 | 0.8548 | 0.8928 | 0.8550 | 0.8928 |
| | $CI$ | ±1.13E−4 | ±1.48E−3 | ±3.32E−4 | ±4.15E−4 | ±1.28E−4 | ±1.21E−4 |
| 3 | $\bar{A}$ | 0.8554 | 0.8931 | 0.8550 | 0.8928 | 0.8550 | 0.8927 |
| | $CI$ | ±6.69E−4 | ±7.20E−4 | ±2.83E−4 | ±1.92E−4 | ±2.39E−5 | ±3.65E−5 |

two additional draughts $T_{1_{FL}} = 3.45$ m and $T_{2_{FL}} = 3.75$ m have been analysed. To ensure compliance with the previous calculations, the same calculation settings have been applied, considering a $GM = 2.00$ m for both additional draughts. For brevity, Table 4 reports only the results for $\bar{A}$ and 95% $CI$, for a direct comparison between EMSA3 and FLARE metrics for cruise vessels. It can be observed that the mean value $\bar{A}$ changes between the two safety metrics. However, the order of magnitude of $CI$ remains almost the same, confirming the $CI$ reduction potential of the enhanced sampling processes. As a matter of fact, the provided example on this test barge shows that the adoption of *SMPL-3* is beneficial to decrease variability in $A$-index calculations, regardless the damage type, the sampling size and the safety metrics adopted.

### 5.2. P-factors analysis

Besides the analysis on the final values of $A$-indices, it is worthy to investigate more in detail the effect of the sampling processes on the $p$-factors. The relative $A_{jk}$ are function of the $p$ and $s$ factors (see Eq. (2)). However, only the $p$-factors are influenced by the sampling process, being $s$-factors an intrinsic characteristic of the hull-form, loading condition and internal layout. Therefore, the survivability index variance reduction granted by enhanced sampling processes derives from the variability of $p$-factors.

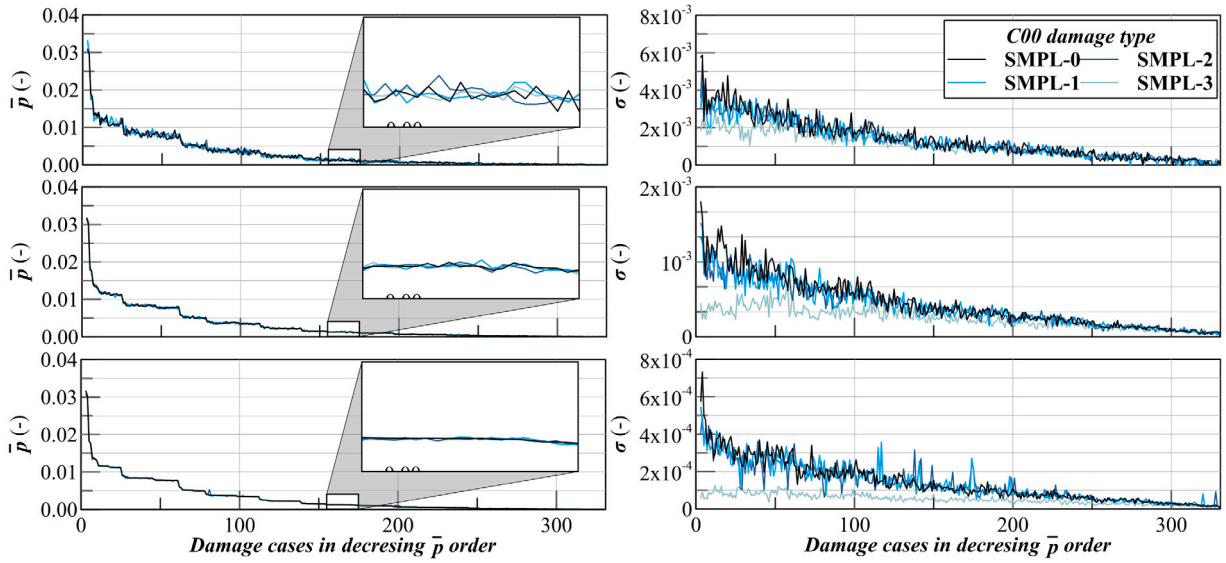


**Fig. 10.** Mean (*left*) and standard deviation (*right*) of C00 damage cases $p$ factors with different sampling processes and sample sizes of $10^3$ (*top*), $10^4$ (*middle*) and $10^5$ (*bottom*) for the test barge at draught $T_1$.

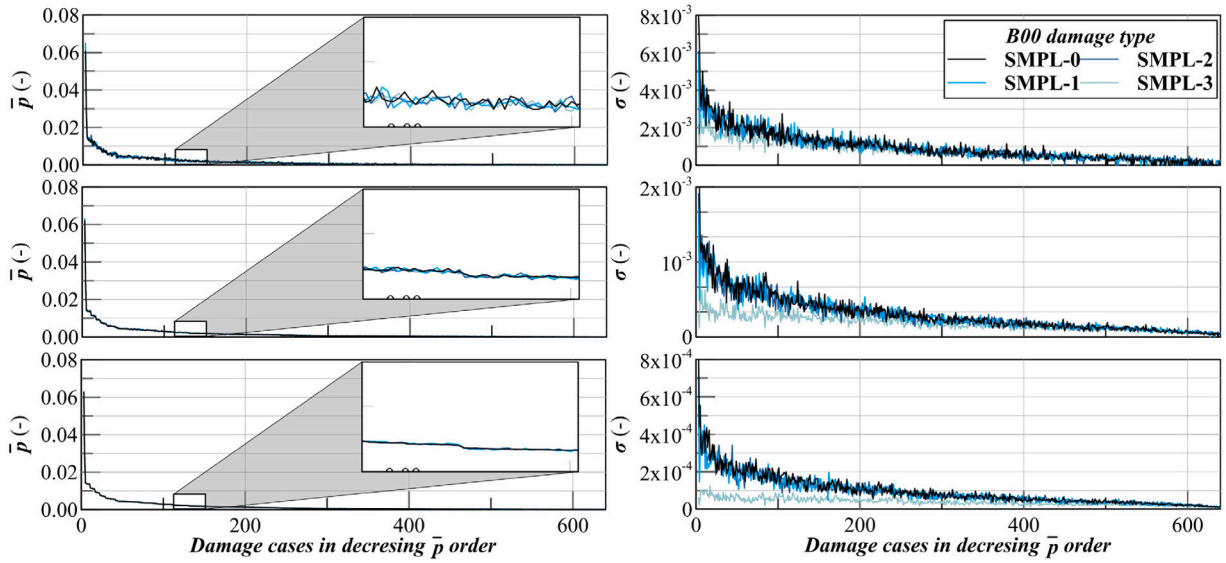


**Fig. 11.** Mean (*left*) and standard deviation (*right*) of B00 damage cases $p$ factors with different sampling processes and sample sizes of $10^3$ (*top*), $10^4$ (*middle*) and $10^5$ (*bottom*) for the test barge at draught $T_1$.

The simple internal layout of the test barge leads to a much lower number of damage cases than a traditional internal layout of a passenger ship. It is then possible to give a more detailed overview of the $p$ values associated to specific damage cases. To this end, all the 20 repetitions performed at each draught have been grouped in such a way to determine $\bar{p}$ and variance $\sigma$ for all the damage cases associated to a specific damage type. As not all the damage cases are present in each sample, the undetected ones have been considered with a $p$ factor equal to 0.0. The present section reports the analysis performed for draught $T_1$, as the same behaviour has been noted for all the tested draughts.

Figs. 10–12 show, for the reference barge at $T_1$, the behaviour of $\bar{p}$ and associated $\sigma$ for the detected damage cases of C00, B00 and S00 damage types, respectively. Each figure contains the results for the three increasing sample sizes of $10^3$, $10^4$ and $10^5$, presenting a curve for each sampling method. For all the reported cases, the ordering of the damage cases derives from the average $\bar{p}$ values of the $10^5$ samplings with *SMPL-0* method, sorting the damages in decreasing order. Due to the differences in the damage characteristic distributions, the three damage types identify different damage cases with different occurrence (i.e. the $p$ factors).

Fig. 10 illustrates the C00 damage types for $T_1$. For such case, the detected unique damages are around 300. The $\bar{p}$ values of all the sampling procedures remain on the same level, regardless the sample size. However, having a look at the magnifier boxes, it is possible to observe that with a sample size of $10^3$ there are value oscillations between the four different sample methods. Increasing $N_s$, $\bar{p}$ values remains almost constant between sample methods, with negligible differences for $N_s = 10^5$. This behaviour for $\bar{p}$ values justifies the small differences observed in the $\overline{A_{jk}}$. However, the $\sigma$ values do not follow the same trend. Observing the results for $N_s = 10^3$, *SMPL-0*, *SMPL-1* and *SMPL-2* have levels for $\sigma$ oscillating around the same values, with *SMPL-1* and *SMPL-2* granting lower $\sigma$ for the most probable cases. *SMPL-3* grants the lowest $\sigma$ values among all the damage cases, with a variance reduction around 50% for the 60 most probable cases. Increasing the sample size, the behaviour remains the same, but *SMPL-3* has an even higher $\sigma$ reduction compared to the other methods.

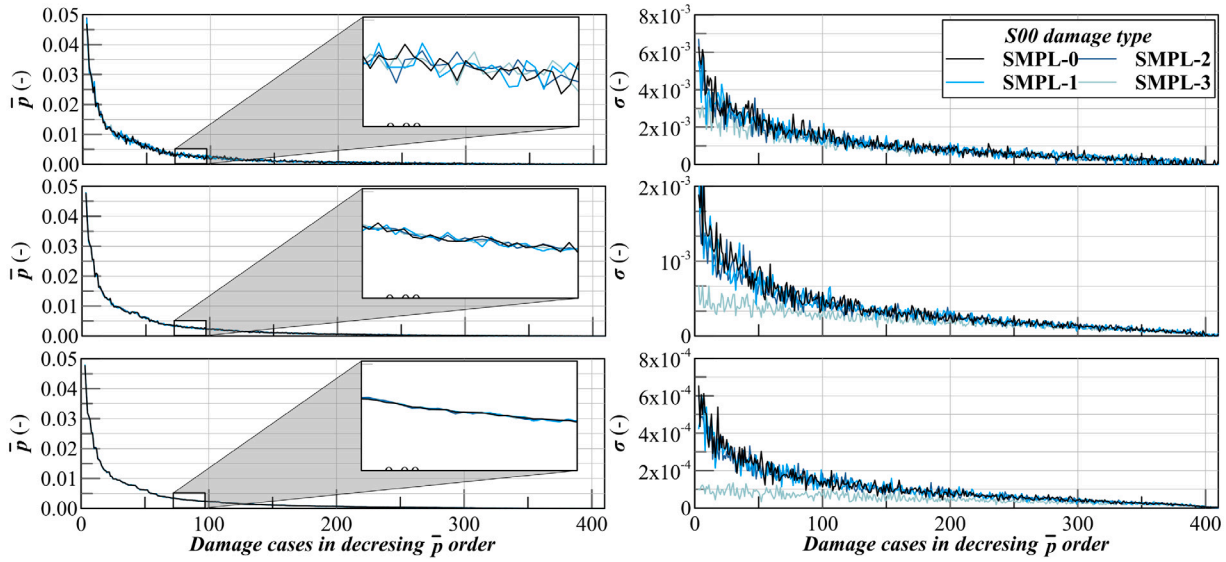


**Fig. 12.** Mean (*left*) and standard deviation (*right*) of S00 damage cases $p$ factors with different sampling processes and sample sizes of $10^3$ (*top*), $10^4$ (*middle*) and $10^5$ (*bottom*) for the test barge at draught $T_1$.

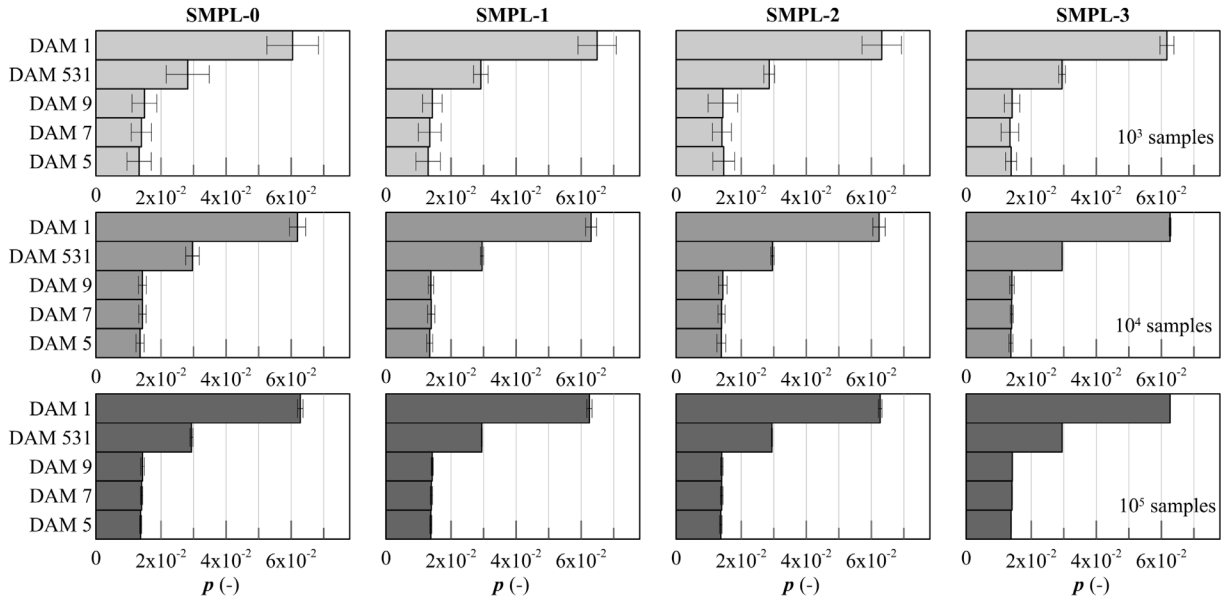


**Fig. 13.** $p$ factor comparison of the five most probable B00 damage cases with different sampling processes and sample sizes of $10^3$ (*top*), $10^4$ (*middle*) and $10^5$ (*bottom*).

The same considerations can be derived also for the B00 and S00 damages, even though the number of unique cases is larger than the C00 ones. Both cases confirm the good $\sigma$ reduction performances of *SMPL-3* method, and a substantial equivalence between *SMPL-1* and *SMPL-2*. Fig. 11 shows that the $\sigma$ values provided by *SMPL-3* for B00 damages, where more than 600 damage cases have been identified, is relevant also for damage cases with low $\bar{p}$ values. This is particularly evident for the $N_s = 10^5$ cases, where the low $\sigma$ are evident for the 400 most probable damage cases, where the $\bar{p}$ value is below $10E-4$. As an additional consideration, it can be observed that, regardless the magnitude of $\bar{p}$, the order of magnitude for $\sigma$ remains the same between the different damages types for constant $N_s$ values.

The presented results allow to have a global vision of the $\bar{p}$ and associated $\sigma$. Fig. 13 gives a more detail overview of the $\bar{p}$ and associated 95% $CI$ on the mean for the five most probable B00 cases at $T_1$. The picture shows that for this specific damage type, the first damage has almost the double probability of occurrence than the second most probable one. This is due to the relatively simple internal layout of the barge in combination with probability definition of the damage characteristics. The consequence is that the most probable damage case (i.e. DAM 1) is the one affecting only the fore double bottom compartment and the second most probable (i.e. DAM 531) affects the aft double bottom room. The figure shows also that the $CI$ (and consequently $\sigma$) for the most probable damages is lower using *SMPL-3*, regardless the sample size. The differences between *SMPL-0*, *SMPL-1* and *SMPL-2* are evident only for the first two most probable cases, where *SMPL-1* and *SMPL-2* have a lower $CI$ compared to *SMPL-0*. Already from the fourth most probable damage case it is not clearly evident which is the method within the three granting the lower variance.

Fig. 14 shows the five less probable B00 damages at $T_1$ according to the $\bar{p}$ ordering of *SMPL-0* cases with $N_s = 10^5$. The figure clearly shows that the decreasing $\bar{p}$ order is not the same for all the sampling procedures, and this reflects more to the damage cases with low occurrence

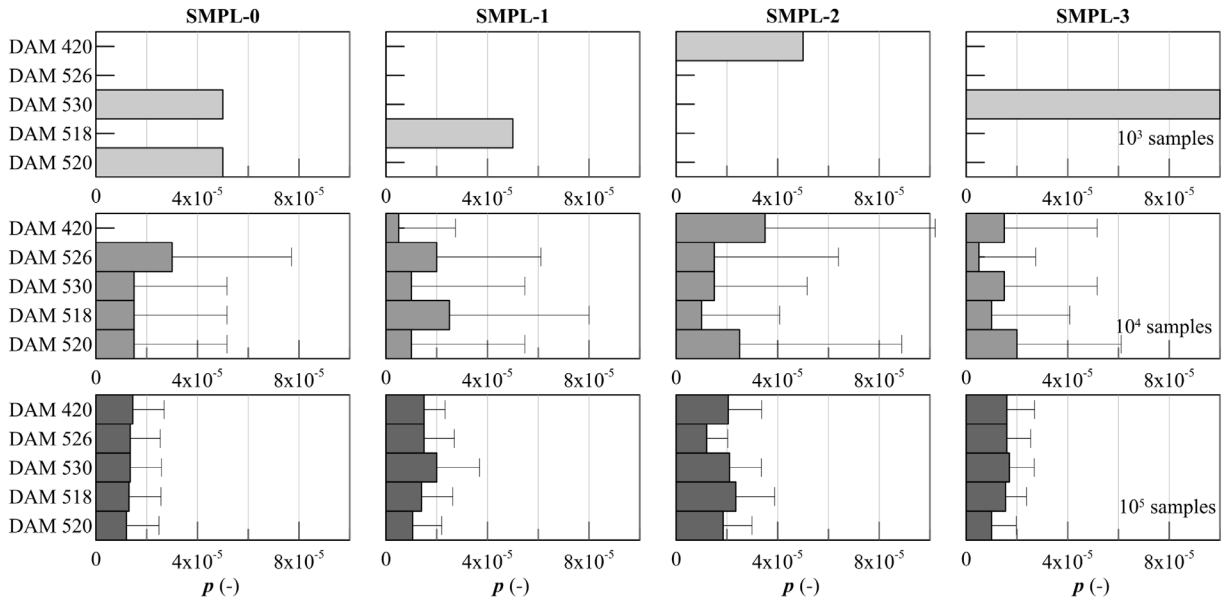


**Fig. 14.** $p$ factor comparison of the five less probable B00 damage cases with different sampling processes and sample sizes of $10^3$ (*top*), $10^4$ (*middle*) and $10^5$ (*bottom*).

rather than the most probable ones. An important highlight of this last comparison is related to the specific $\overline{p}$ of low probability damages. With a sampling size of $10^3$, the identified cases with lower occurrence have a $\overline{p} = 5 \cdot 10^{-5}$ for *SMPL-0*, *SMPL-1* and *SMPL-2*, meaning that the damage case was detected only in one of the 20 repetitions. For *SMPL-3* the identified case within the reported set has been recursively found 10 times in the 20 repetitions. It appears that *SMPL-0* highlight the same problem also for an $N_s = 10^4$. However, the evident differences found in the $\overline{p}$ ordering does not allow to clearly analyse the effective capability of the four procedures to identify unique cases.

### 5.3. Identification of unique damage cases

The $p$-factors analysis highlighted that the variability of the damage cases with low occurrence was also influenced by the fact that some cases were not detected through the 20 consecutive repetitions. The trend is more evident for *SMPL-0* method, and appears through all the tested $N_s$ groups of simulations. *SMPL-1* and *SMPL-2* highlight this mostly for low sample sizes and *SMPL-3* only at low $N_s$ values.

A dedicated analysis has been performed to clearly identify the unique cases detected by the four implemented sampling processes among the 20 repetitions. Fig. 15 shows the number of unique cases detected for C00, B00 and S00 damage types using the four different sampling procedures and the sampling sizes of $10^3$, $10^4$ and $10^5$. The data refers to loading condition $T_1$, but the same trends have been observed for the other draughts. For this loading condition the real number of unique cases is 328 for C00, 640 for B00 and 410 for S00. From the data, it is evident that the sample size $N_s$ strongly influences the number of unique cases detected in a single repetition, with major impact for B00 and S00 damage types.

Considering C00 damages and $N_s = 10^3$, the mean number of unique cases detected by *SMPL-0* method is 208 per repetition; *SMPL-1* and *SMPL-2* detect 205 cases, and *SMPL-3* detects 213 ones. Increasing the $N_s$ to $10^4$, *SMPL-0*, *SMPL-1* and *SMPL-2* detect a mean of 300 unique cases; *SMPL-3* 305. For the higher sample size, all methods detect around 327 and 328 unique cases. For B00 damages the relative differences between sample sizes and methods are higher compared to C00 damage type. *SMPL-0* identifies a mean of 301, 554 and 636 unique cases per run by increasing the sample size, 303, 556 and 637 for *SMPL-1*, 305, 555 and 636 for *SMPL-2*, and 320, 567 and 638 for *SMPL-3*. S00 damages have a trend similar to B00 damage type, where

**Table 5**
Unique cases detection through consecutive $N_r$ repetitions for the test barge at loading condition $T_1$.

| | $N_r$ | SMPL-0 | | | SMPL-1 | | | SMPL-2 | | | SMPL-3 | | |
|---|---|---|---|---|---|---|---|---|---|---|---|---|---|
| | | $N_s$ | | | $N_s$ | | | $N_s$ | | | $N_s$ | | |
| | | $10^3$ | $10^4$ | $10^5$ | $10^3$ | $10^4$ | $10^5$ | $10^3$ | $10^4$ | $10^5$ | $10^3$ | $10^4$ | $10^5$ |
| C00 | 1 | 212 | 303 | 328 | 203 | 296 | 328 | 210 | 289 | 327 | 207 | 305 | 328 |
| | 5 | 279 | 324 | 328 | 276 | 324 | 328 | 276 | 322 | 328 | 281 | 325 | 328 |
| | 10 | 297 | 326 | 328 | 301 | 326 | 328 | 301 | 327 | 328 | 297 | 326 | 328 |
| | 20 | 315 | 328 | 328 | 312 | 328 | 328 | 315 | 328 | 328 | 315 | 328 | 328 |
| B00 | 1 | 307 | 565 | 635 | 310 | 557 | 639 | 300 | 547 | 639 | 318 | 565 | 638 |
| | 5 | 488 | 626 | 640 | 495 | 626 | 640 | 497 | 628 | 640 | 496 | 624 | 640 |
| | 10 | 550 | 635 | 640 | 554 | 635 | 640 | 560 | 640 | 640 | 560 | 635 | 640 |
| | 20 | 594 | 639 | 640 | 601 | 639 | 640 | 597 | 640 | 640 | 599 | 639 | 640 |
| S00 | 1 | 190 | 337 | 394 | 195 | 339 | 393 | 200 | 334 | 394 | 202 | 346 | 394 |
| | 5 | 294 | 385 | 401 | 299 | 384 | 404 | 298 | 385 | 404 | 317 | 389 | 404 |
| | 10 | 340 | 390 | 406 | 346 | 397 | 407 | 342 | 392 | 407 | 346 | 396 | 407 |
| | 20 | 354 | 401 | 409 | 366 | 404 | 410 | 365 | 396 | 409 | 373 | 400 | 410 |

*SMPL-0* identifies a mean of 203, 334 and 395 unique cases per run by increasing the sample size, 200, 342 and 395 for *SMPL-1*, 202, 340 and 395 for *SMPL-2*, and 208, 347 and 395 for *SMPL-3*. From the analysis of the results it can be stated that *SMPL-3* method is capable to detect always about 4% more unique cases in single repetitions than the standard sampling method *SMPL-0*. *SMPL-1* and *SMPL-2* have capabilities comparable with *SMPL-0*.

The first step of the analysis refers only to unique cases detected in each repetition. However, the unique cases detected through consecutive iterations are not always the same. Therefore, it is necessary to identify the unique cases detected through consecutive repetitions.

Table 5 reports the number of unique cases considering 1, 5, 10 and 20 repetitions. For C00 damage types all the procedures show the same capability for unique case prediction, being capable to identify a maximum number of 328 cases when the total amount of samplings is about $10^5$. B00 damages behave in a different way. The total amount of unique cases is higher than C00 ones, reaching a maximum of 640 cases when the global sampling size is around $5 \cdot 10^5$. However, the additional cases detection trend changes with the sample method, with *SMPL-3* being able to detect more unique cases with low samples compared to the others. For S00 damage type, a maximum number of 410 cases is identified only with a global sample size bigger than $10^6$. As for B00

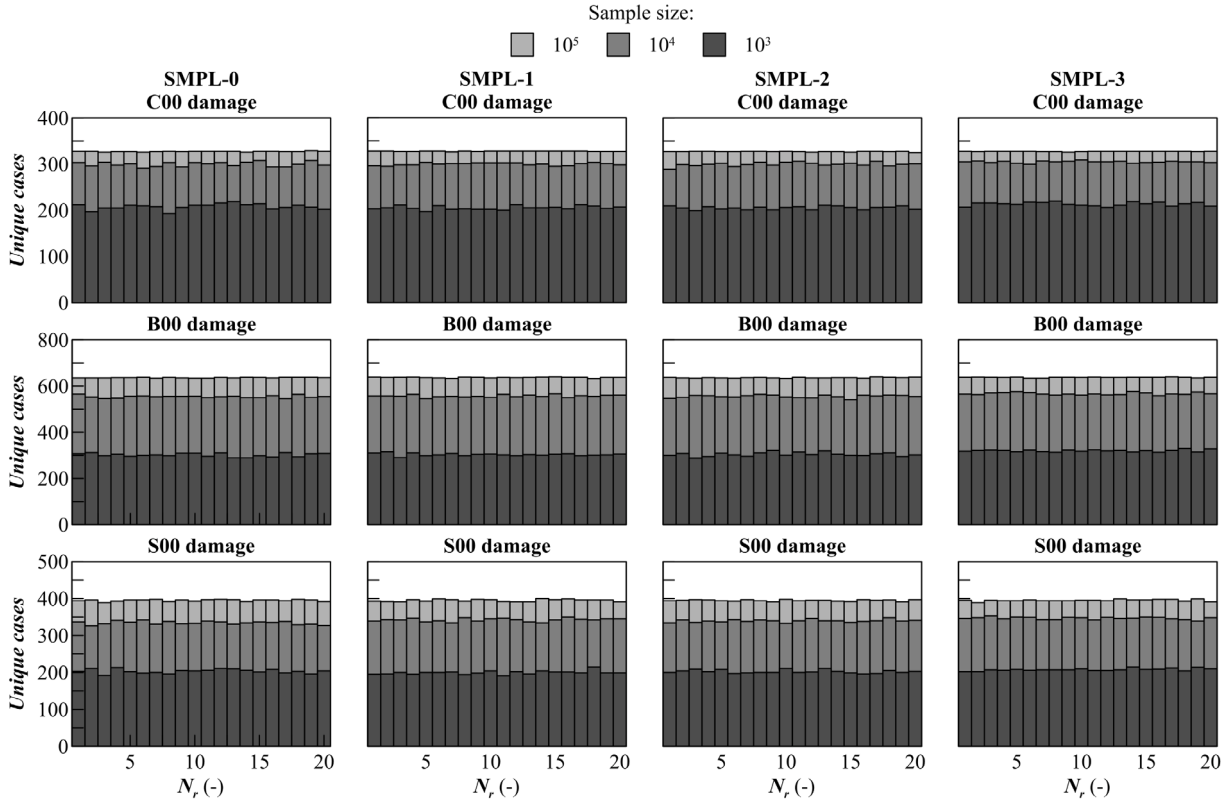


**Fig. 15.** Unique cases detected by the four different sampling procedure for the reference barge at loading condition $T_1$.

cases, *SMPL-3* allows detecting a higher number of cases with a small sample size. In any case, benefits decrease at higher $N_r \cdot N_s$ values, where all sampling procedures identify all unique cases for the tested barge.

These considerations demonstrate an additional potential benefit of *SMPL-3* method for low sample sizes. In fact, besides variance reduction on *p*-factors, *SMPL-3* identifies more unique cases with lower sample size, increasing the confidence for the obtained *A*-index while using such a sampling process.

### 5.4. Ranking of the proposed sampling methods

The extensive analysis performed on the presented test barge enables a ranking between the four sampling procedures for the presented case. According to the provided analyses, a final ranking can be summarised as follows:

1. *SMPL-3*: this sampling process, based on multidimensional LD sequences, is without any doubt the most promising method to reduce variability for *A*-index calculation on the reference barge. The method shows very good performances in the variance reduction of *p*-factors both for low and high sample sizes. Moreover, with low $N_s$ values it is capable to identify more unique cases than other procedures with the same number $N_r$ of repetitions.
2. *SMPL-1* and *SMPL-2*: the procedure based on LH approach and the one using mono-dimensional LD sequences show almost the same potential on the tested case. The two procedures have comparable variability for the *A*-index calculation that in any case is better compared to standard MC method, but not enough to be equivalent with *SMPL-3* benefits.
3. *SMPL-0*: the standard sampling method currently used in the calculation framework for damage stability has the highest variability compared to other procedures. The performances of the sampling process, both in terms of variability on repetitions and detection of unique cases, are comparable with *SMPL-1* and *SMPL-2* only with an high $N_s$ number. In any case, performances are always lower than *SMPL-3* method.

The computational effort required by the different sampling methods is equivalent between the four processes, giving no additional preference to one of the methods.

Besides the indication given on the presented barge, this study allows to identify the potentials of different sampling process, and in particular of *SMPL-3* method, for the damage stability assessment of a passenger ship. In fact, the capability of detecting a higher number of unique cases with relatively lower $N_s$ values could be a plus for more complex internal layouts, as the one of passenger ships, trying to reduce the amount of calculations.

## 6. Implication for damage stability assessment on a passenger ship

The study performed on the reference barge shows that the RQMC sampling method based on a multidimensional Sobol sequence (*SMPL-3*) gives the best benefits in lowering the dispersion of *A*-index data and the detection of unique damage cases. Therefore, the potential of this sampling strategies are here tested on a complex geometry to evaluate the possible benefits of such a process on a real cruise-ship internal layout.

To this end, use is made of a sample ship available in project FLARE, and, to further check the potential of the detection of unique cases, a more granular subdivision is here considered, modelling internal spaces more accurately than conventional static calculations. Table 6 shows the main particulars of the cruise vessel and Fig. 16 the internal layout modelled for the calculations, resulting in 364 distinct rooms (about double the conventional static calculations on the reference ship). The calculations considers all the rooms as watertight, neglecting flooding

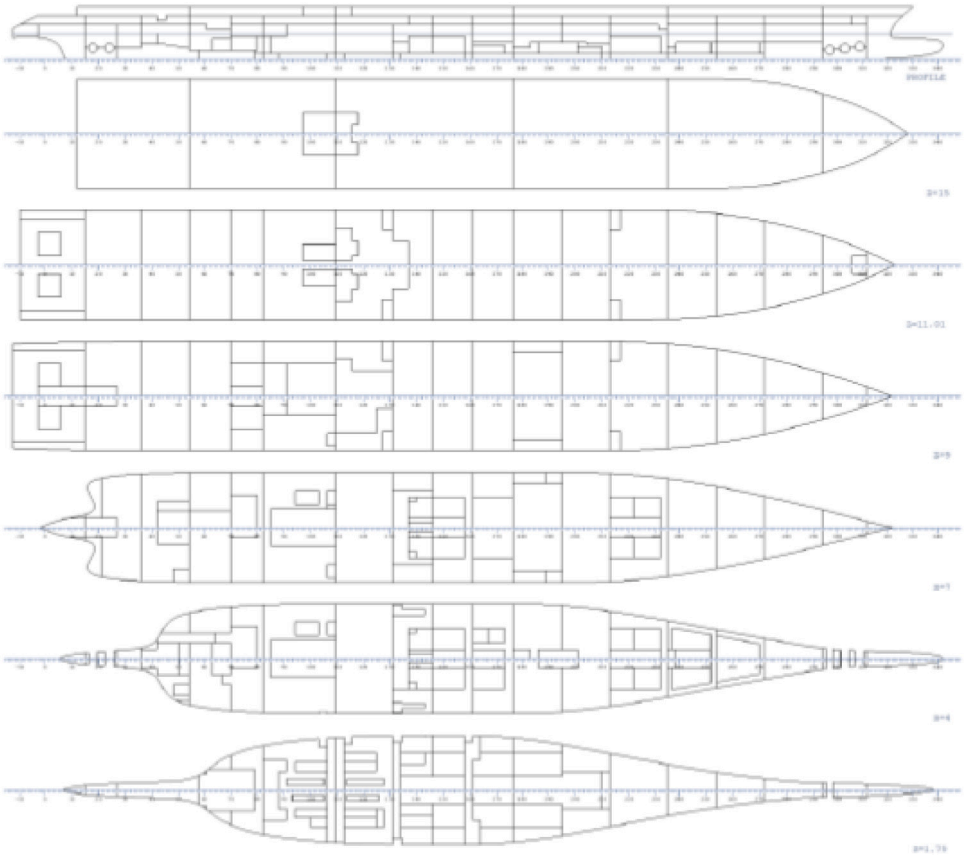

**Fig. 16.** Sample cruise-ship internal layout used to test the sampling process.

**Table 6**
Sample cruise-ship main particulars.

| Quantity | | Value | Unit |
|---|---|---|---|
| Length over all | $L_{OA}$ | 300.00 | m |
| Length between perpendiculars | $L_{BP}$ | 270.00 | m |
| Subdivision length | $L_s$ | 296.74 | m |
| Breadth | $B$ | 35.20 | m |
| Gross tonnage | $GT$ | 95,900 | – |
| Lower subdivision draught | $T_1$ | 7.65 | m |
| Partial subdivision draught | $T_2$ | 7.98 | m |
| Deepest subdivision draught | $T_3$ | 8.20 | m |
| Metacentric height at $T_1$ | $GM_{T_1}$ | 2.45 | m |
| Metacentric height at $T_2$ | $GM_{T_2}$ | 2.88 | m |
| Metacentric height at $T_3$ | $GM_{T_3}$ | 3.49 | m |

stages not implemented in PROTEUS3 software. As the internal layout is not the same used for SOLAS assessment of static damage stability, the resulting values for $A$ indices are purely indicative and conservative compared to traditional analyses. This is not an issue, as the study is related to the variability of the index and not on its determination.

The main target of this study is the identification of the potential reduction of sample size and repetition that can be achieved by applying *SMPL-3* on a complex layout. Previous studies (Bulian et al., 2016, 2019) identify as practical acceptable level of accuracy for $A$-index the one obtained with *SMPL-0* method with $N_s = 10^4$ and $N_r = 5$, meaning a total of 50,000 sampled breaches. Here, this sample size has been applied to the detailed cruise-ship layout, adopting both *SMPL-0* and *SMPL-3* method to C00, B00 and S00 damage types, for the three SOLAS draughts reported in Table 6.

Table 7 reports the partial $A_{jk}$ indices obtained for the tested conditions in terms of mean value and 95% confidence interval on the mean. Table 7 collects also the mean values for indices $A_k$ (obtained from Eq. (16)) and the total $A$ (using eSAFE safety metrics reported in Table 1) with the associated $CI$. Considering the 5 repetitions of $10^4$ samples with both sampling methods, the mean values of the obtained partial and global indices does not change, having discrepancies of less than 0.5%. However, the associated 95% $CI$ are different. Considering the partial indices $A_{jk}$ and the partial $A_k$ for the different damage types, it results that *SMPL-3* method provides $CI$ intervals that are from 3 to 5 times smaller than the ones obtained with *SMPL-0*. When partial indices are summed together to obtain the total $A$, the $CI$ resulting from *SMPL-0* reduces, remaining, in any case, about 2 times higher than the one resulting from *SMPL-3* method.

The application on a complex internal layout confirms the trend observed for the simplified barge geometry, highlighting that *SMPL-3* method is capable to reduce the variability of $A$-index compared to standard MC sampling. The same is also for the unique cases detection. As an example, for the true complex layout at $T_1$, the adoption of *SMPL-3* allows detecting 6926 C00 types unique cases among the 5 repetitions, with an average number of 3100 unique cases per single repetition. The standard *SMPL-0* method identifies 6710 unique cases, with an average of 2980 cases per repetition. Same trend is observed also for other damage types, with *SMPL-3* method always capable to detect from 3 up to 5% more unique cases than *SMPL-0* process, resulting in 10395 unique B00 cases (against 9984 given by *SMPL-0*) and 5954 unique S00 cases (5753 for *SMPL-0*). Comparable values are observed also for other draughts.

### 6.1. Sample size reduction

Having with *SMPL-3* the capability to reduce to almost a half the CI% on the total $A$-index, it is then possible to identify what is the limit for the tested case at which the sample size and repetitions could be reduced by keeping the same CI% provided by *SMPL-0*. To this end, different possible strategies can be pursued:

**Table 7**
$A_{jk}$, $A_k$ and $A$ values for the sample cruise-ship case.

| | | SMPL-0 | | | | SMPL-3 | | | |
|---|---|---|---|---|---|---|---|---|---|
| | | $T_1$ | $T_2$ | $T_3$ | $\sum_j$ | $T_1$ | $T_2$ | $T_3$ | $\sum_j$ |
| C00 | $\overline{A_{jk}}, \overline{A_k}$ | 0.9318 | 0.8585 | 0.8295 | 0.8615 | 0.9298 | 0.8560 | 0.8329 | 0.8615 |
| | $CI$(95%) | ±2.98E−3 | ±3.21E−3 | ±2.77E−3 | ±1.61E−3 | ±8.03E−4 | ±5.24E−4 | ±7.73E−4 | ±4.06E−4 |
| B00 | $\overline{A_{jk}}, \overline{A_k}$ | 0.9780 | 0.9711 | 0.9691 | 0.9717 | 0.9765 | 0.9709 | 0.9686 | 0.9711 |
| | $CI$(95%) | ±2.05E−3 | ±2.26E−3 | ±2.09E−3 | ±9.99E−4 | ±3.99E−4 | ±5.51E−4 | ±5.55E−4 | ±2.95E−4 |
| S00 | $\overline{A_{jk}}, \overline{A_k}$ | 0.9066 | 0.8740 | 0.8605 | 0.8751 | 0.0.9062 | 0.8729 | 0.8595 | 0.8742 |
| | $CI$(95%) | ±2.09E−3 | ±1.18E−3 | ±4.14E−3 | ±1.24E−3 | ±6.17E−4 | ±4.89E−4 | ±3.15E−4 | ±2.49E−4 |
| Total | $\overline{A}$ | 0.8901 | | | | 0.8894 | | | |
| | $CI$(95%) | ±4.21E−4 | | | | ±1.98E−4 | | | |

**Table 8**
$A_{jk}$, $A_k$ and $A$ values for the sample cruise-ship case with $N_s = 5 \cdot 10^3$.

| | | SMPL-3 | | | |
|---|---|---|---|---|---|
| | | $T_1$ | $T_2$ | $T_3$ | $\sum_j$ |
| C00 | $\overline{A_{jk}}, \overline{A_k}$ | 0.9302 | 0.8548 | 0.8333 | 0.8613 |
| | $CI$(95%) | ±1.02E−3 | ±7.81E−4 | ±1.04E−3 | ±6.66E−4 |
| B00 | $\overline{A_{jk}}, \overline{A_k}$ | 0.9767 | 0.9712 | 0.9682 | 0.9711 |
| | $CI$(95%) | ±8.23E−4 | ±5.42E−4 | ±4.95E−4 | ±3.14E−4 |
| S00 | $\overline{A_{jk}}, \overline{A_k}$ | 0.9060 | 0.8721 | 0.8591 | 0.8737 |
| | $CI$(95%) | ±5.96E−4 | ±4.38E−4 | ±1.05E−3 | ±4.77E−4 |
| Total | $\overline{A}$ | 0.8891 | | | |
| | $CI$(95%) | ±1.17E−4 | | | |

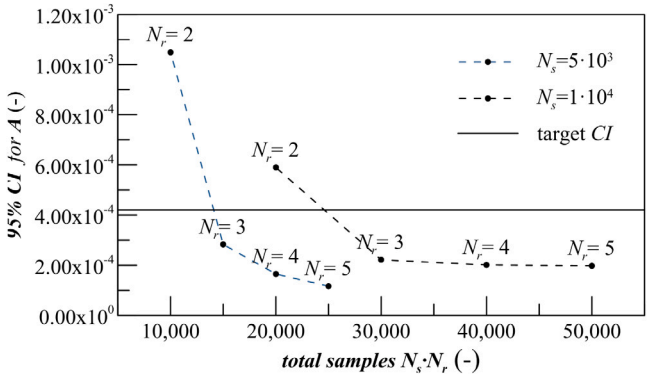


**Fig. 17.** $CI$ variations for total $A$-index against target value changing $N_s$ and $N_r$ using *SMPL-3*.

1. reduce the number of repetition $N_r$ while keeping $N_s$ constant;
2. reduce $N_s$ while keeping $N_r$ constant;
3. reduce both $N_s$ and $N_r$.

The first option can be checked with the set of data used to produce the analyses reported in Table 7. The other two options require the execution of additional calculations. Therefore, an ulterior set of samplings has been produced considering 5 repetitions with $N_s = 5 \cdot 10^3$, adopting *SMPL-3* method only. Table 8 shows the obtained partial and total $A$ indices mean and $CI$. It can be observed that the mean values of partial and total indices is comparable with the one resulting from the original samples with $N_s = 10^4$, registering variations of less than 0.1%. Therefore, only $CI$ values change significantly between Tables 8 and 7 for *SMPL-3* results.

Fig. 17 summarises the results that can be achieved in terms of total samples reduction, always considering the $CI$ value given by MC procedure with $N_r = 5$ and $N_s = 10^4$ as reference target. By reducing the number of repetitions, the associated $CI$ increases, as, keeping in mind Eq. (3), the value of $t$ increases, $N_r$ decreases and $\sigma$ varies according to the sample. Keeping $N_s = 10^4$ allows to reduce $N_r$ to 3, having always a lower $CI$ compared to the target one. Changing $N_s$ to $5 \cdot 10^3$, the condition with $N_r = 5$ gives a lower $CI$ than the target one. Also for this case, reducing $N_r$ to 3 allows maintaining the $CI$ under the target value. Therefore, from this analysis results that, for the given geometry, the *SMPL-3* method could give the same confidence interval on the total $A$-index of a conventional MC sampling, using 15,000 breaches instead of 50,000 per each loading condition and damage type.

However, a reduction of the total number of samples implies a reduction in the total number of unique cases detected. Reducing $N_s$ from $10^4$ to $5 \cdot 10^3$, the total amount of damage cases detected is 35% lower. With the mean values of the $A$ indices not that much sensitive to $N_s$ change suggests that the additional cases have marginal $p$ values compared to the initially predicted ones. Being more conservative and considering the 3 repetitions with $N_s = 10^4$ as final choice for the $A$-index determination reduces the breaches to 30,000, but the global reduction of unique cases is around 12% for the given geometry.

Both the breaches reduction ratios are a significant improvement compared to standard MC sampling and actual state-of-art calculations in damage stability. However, further investigations are needed on a wider set of ships to verify the effective lower breaches limits applicable by using *SMPL-3* method. In any case, the results shown for the barge and the sample cruise-ships highlight that *SMPL-3* is a valid alternative to the conventional MC sampling for damage sampling in a probabilistic framework.

## 7. Conclusions

The present work gives a comprehensive overview of the sampling process used in the probabilistic framework for damage stability assessment of passenger ships. The sampling process of damages within the SOLAS probabilistic framework has been analysed, proposing three alternative sampling processes useful to reduce uncertainties and $A$-index variability while adopting a non-zonal approach. The present paper compares the performances of LH and RQMC sampling with standard MC approach. The test case for collision, bottom and side grounding damages on a simple reference barge, highlights how the RQMC method based on multi-dimensional Sobol sequences (*SMPL-3*) gives more benefits than other procedures in the reduction of variability for partial and total $A$-indices. A detailed analysis on the evaluated $p$-factors highlights that the reduction of variability in $A$ is strongly related to the reduction of $\sigma$ for the $p$ values evaluated per each unique damage case among multiple repetitions. Moreover, *SMPL-3* method is capable to detect a higher number of unique damage cases compared to other methods. Therefore, it could significantly reduce the number of samples to be generated to achieve a target confidence level on the results.

The benefits provided by *SMPL-3* have been further highlighted testing the sampling process on a complex internal layout, more granular than traditional geometries used for static calculations. Comparing results with traditional MC sampling, it has been found that *SMPL-3* method grants the same $CI$ on the final $A$-index using about 1/3 of the total breach samples. However, to clearly identify a suitable

lower limit for the sample size needed to evaluate *A*-index, a more extensive study on a wider number of ships with different size is needed. Nevertheless, the results on the reference barge and on the sample cruise-ship indicate that the adoption of *SMPL-3* method could be really effective with different internal layouts and size.

The same procedure, can be extended also for dynamic analysis, where the benefits in terms of calculation reduction could be even higher than for static calculations, and are going to be addressed by the authors in further studies. The reduction of the number of breaches to be generated to reach a reasonable convergence level for the *A*-index is a significant improvement for the practical engineering application of damage stability.

## CRediT authorship contribution statement

**Francesco Mauro:** Conceptualizaton, Methodology, Software, Investigation, Writing – original draft, Writing – review & editing. **Dracos Vassalos:** Conceptualizaton, Writing – review & editing, Supervision.

## Declaration of competing interest

The authors declare that they have no known competing financial interests or personal relationships that could have appeared to influence the work reported in this paper.

## Acknowledgements

The financial support of the EU project FLARE is acknowledged. The information and views set out in this paper are those of the authors and do not necessarily reflect the official opinion of all FLARE partners.

## References

Atzampos, G., Vassalos, D., Cichowicz, J., Paterson, D., Boulougouris, E., 2019. ESAFE - cruise ship survivability in waves. In: 17th International Ship Stability Workshop. Helsinki, Finland, pp. 265–274.

Bradley, P., Fox, B., 1988. Algorithm 659: implementing Sobol's quasi random sequence generator. ACM Trans. Math. Software 14 (1), 88–100.

Bulian, G., Cardinale, M., Dafermos, G., Eliopoulou, E., Francescutto, A., Hamann, R., Lindroth, D., Luhmann, H., Ruponen, P., Zaraphonitis, G., 2019. Considering collision, bottom grounding and side grounding/contact in a common non-zonal framework. In: 17th International Ship Stability Workshop. Helsinki, Finland, pp. 245–257.

Bulian, G., Cardinale, M., Dafermos, G., Lindroth, D., Ruponen, P., Zaraphonitis, G., 2020. Probabilistic assessment of damaged survivability of passenger ships in case of grounding or contact. Ocean. Eng. 218, 107396.

Bulian, G., Francescutto, A., 2010. Probability of flooding due to grounding damage using a p-factor formulation. GOALDS Project.

Bulian, G., Lindroth, D., Ruponen, P., Zaraphonitis, G., 2016. Probabilistic assessment of damaged ship survivability in case of grounding: development and testing of a direct non-zonal approach. Ocean. Eng. 120, 331–338.

Cools, R., Nuyens, D., 2014. Monte Carlo and Quasi-Monte Carlo Methods. Springer.

Cranley, R., Patterson, T., 1976. Randomization of number theoretic mehods for multiple integration. SIAM J. Numer. Anal. 13, 904–914.

FLARE, 2019-2022. Flooding Accident Response, Vol. 2. EU H2020 - MG2.

Hammersley, J., Handscomb, D., 1964. Monte Carlo Methods. Methuen & co LTD.

IMO, 2006. Resolution MSC.216(82) - Amendments to the International Convention for the Safety of Life at Sea 1974, as amended, 8 December. International Maritime Organisation.

IMO, 2017. Resolution MSC.421(98) - Amendments to the International Convention for the Safety of Life at Sea 1974, as amended, 15 June. International Maritime Organisation.

IMO, 2020. International Convention for the Safety of Life at Sea (SOLAS). Consolidated Edition as of 2020. International Maritime Organisation.

Jaeckel, P., 2002. Monte Carlo Methods in Finance. John Wiley & Sons, New York, NY.

Jasionowski, A., 2001. An Integrated Approach to Damage Ship Survivability Assessment (Ph.D. thesis). University of Strathclyde.

Krüger, S., Dankowski, H., 2019. A Monte Carlo based simulation method for damage stability problems. In: ASME 2019 38th International Conference on Ocean, Offshore and Artic Engineering (OMAE 2019).

Krüger, S., Kehren, F., Dankowski, H., 2008. Leckstabilitätsberechnungen durch Monte Carlo simulationen. Festschr. Schiftenreiche Shiffbau 641, 60–85, in German.

L'Ecuyer, P., Lemieux, C., 2002. Recent Advances in Randomized Quasi-Monte Carlo Methods. Kluwer Academic Publisher, Boston, MA, pp. 419–478, chapter Modelling Uncertainties: An Examination of Stohastic Theory, Methods and Applications.

Levitan, Y., Markovich, N., Rozin, S., Sobol, I., 1988. On quasi-random sequences for numerical calculations. USSR Comput. Math. Math. Phys. 28 (5), 755–759.

Lützen, M., 2001. Ship Collision Damage (Ph.D. thesis). Department of Mechanical Engineering, Maritime Engineering, Technical University of Denmark, Lyngby.

Lützen, M., 2002. Damage distributions. HARDER Document 2-22-D-2001-01-4 (version:4, date: 2002-07-29).

Matušek, J., 1998. On the L2-discrepancy for anchored boxes. J. Complexity 14, 527–556.

Mauro, F., Paterson, D., Michalec, R., Boulougouris, E., Vassalos, D., 2021. A damage sampling method to reduce A-index standard deviation in the probabilistic assessment of ship survivability using a non-zonal approach. In: 1st International Conference on the Stability and Safety of Ships and Ocean Vehicles. Glasgow, Scotland, UK.

McKay, M., Beckman, R., Conover, W., 1979. A comparison of three methods for selecting values of input variables in the analysis of output from a computer code. Technometrics 21 (2), 39–45.

Niederreiter, H., 1987. Point sets and sequencies with small discrepancy. Mon.hefte Math. 104, 273–337.

Niederreiter, H., 1988. Low-discrepancies and low-dispersion sequencies. J. Number Theory 30, 51–70.

Niederreiter, H., 1992. Random Number Generation and Quasi-Monte Carlo Methods. SIAM, Philadelphia, PA.

Owen, A., 1997. Monte Carlo variance of scrambled equidistribution quadrature. SIAM J. Numer. Anal. 34 (5), 1884–1910.

Papanikolaou, A., Eliopoulou, E., 2008. On the development of the new harmonised damage stability regulations for dry cargo and passenger ships. Reliab. Eng. Syst. Saf. Saf. Marit. Transp. 93, 1305–1316.

Papanikolaou, A., Spanos, D., Boulougouris, E., Eliopoulou, E., Alissafaki, A., 2004. Investigation into the sinking of the Ro-Ro passenger ferry Express Samina. Int. Shipbuild. Prog. 51, 95–120.

Pawlowski, M., 2004. Subdivision and Damaged Stability of Ships. Euro-MTEC book series, Gdansk, Poland.

Ruponen, P., Linderoth, D., Routi, A.-L., Aartovaara, M., 2019. Simulation-based analysis method for ship survivability of passenger ship. Ship Technol. Res. 63 (3), 182–194.

Sobol, I., Asotky, D., Krenin, A., Kucherenko, S., 2011. Construction and comparison of high-dimensional Sobol'generators. Wilmott J. 64–79.

Spanos, D., Papanikolaou, A., 2014. On the time for the abandonment of flooded passenger ships due to collision damages. J. Mar. Sci. Technol. 19, 327–337.

Tuffin, B., 1996. On the Use of Low Discrepancy Sequences in Monte Carlo Mehods. Technical Report, I.R.I.S.A., Rennes, France.

Vassalos, D., 2008. Risk-Based Ship Design. Springer, pp. 17–98, chapter 2: Methods, Tools and Application.

Vassalos, D., 2020. The role of damaged ship dynamics in addressing the risk of flooding. Ship Offshore Struct. 1–25.

Vassalos, D., Mujeeb-Ahmed, M.-P., 2021. Conception and evolution of the probabilistic methods for ship damage stability and flooding risk assessment. JMSE 1–25.

Wendel, K., 1960. Die wahrscheinlichkeit des überstehns von verletzungen. Shiffstechnik 36 (7), 47–61, in German.

Zaraphonitis, G., Bulian, G., Hamann, R., Eliopoulou, E., Cardinale, M., Luhman, H., 2017. ESAFE-D2.2.1 - description of methodology. Joint Industry Project eSAFE, 29 March (Rev.2).

Zaraphonitis, G., Bulian, G., Lindroth, D., Hamann, R., Luhmann, H., Cardinale, M., Routi, A.-L., Bertin, R., Harper, G., 2015. Evaluation of Risk from Raking Damages due to Grounding. Final Report. DNVGL Report 2015-0168 Rev. 2, Project EMSA/OP/10/2013. Technical Report, European Maritime Safety Agency.